OPTIMIZATION AND EVALUATION OF MANUFACTURING TOLERANCES OF A THREE-MIRROR ASPHERIC CAMERA

by

John Anthony Van Workum

A Thesis Submitted to the Faculty of the

DEPARTMENT OF OPTICAL SCIENCES

In Partial Fulfillment of the Requirements
For the Degree of

MASTER OF SCIENCE

In the Graduate College

THE UNIVERSITY OF ARIZONA

1 9 7 0

STATEMENT BY AUTHOR

This thesis has been submitted in partial fulfillment of requirements for an advanced degree at The University of Arizona and is deposited in the University Library to be made available to borrowers under rules of the Library.

Brief quotations from this thesis are allowable without special permission, provided that accurate acknowledgment of source is made. Requests for permission for extended quotation from or reproduction of this manuscript in whole or in part may be granted by the head of the major department or the Dean of the Graduate College when in his judgment the proposed use of the material is in the interests of scholarship. In all other instances, however, permission must be obtained from the author.

SIGNED: John A. Van Workum

APPROVAL BY THESIS DIRECTOR

This thesis has been approved on the date shown below:

A. B. Meinel
Dr. A.B. MEINEL
Professor and Chairman
of Optical Sciences

2 Jan 1970
Date

PREFACE

The purpose of this study is to determine the practicability of constructing a large aperture, three mirror lens system. The two practical problems which are considered are sky baffling and manufacturing errors. If the system cannot be sky baffled, or if minute fabrication errors greatly degrade the image, construction of the system should not be attempted. During the study, it was found to be necessary to design the system around the sky baffling requirement in order to arrive at an optimum design. The procedure which was used is included in this study. A method of determining a design's sensitivity to manufacturing errors is also presented. These two practical problems must be considered before construction of an expensive lens can begin.

The author wishes to express his sincerest thanks to Mr. Gary Wilkerson for his assistance in completing the designs of several mirror systems. He also wishes to thank Professor Aden B. Meinel and the other members of the Committee of Optical Sciences for their guidance in the preparation of this thesis.

TABLE OF CONTENTS

TABLE OF CONTENTS--Continued

LIST OF ILLUSTRATIONS

LIST OF ILLUSTRATIONS--Continued

LIST OF ILLUSTRATIONS--Continued

LIST OF TABLES

ABSTRACT

In an attempt to design a three-mirror aspheric camera, a procedure was developed to arrive at a design with a minimum obscuration ratio. It was found that, in some cases, the sky baffling became the diffracting obscuration rather than the obscuration caused by the secondary. The procedure allowed for this and was able to select a system with the smallest diffracting obscuration in the pupil.

Initially, two designs were selected and optimized through the use of aspheric surfaces. The designs represented two extremes in that one had much faster surfaces than the other. The fast mirror system was easier to optimize, performed better, and had the shorter overall length.

Further, evaluation of manufacturing errors on the fast mirror design showed that an acceptable level of performance could be expected if the errors were kept small. The maximum errors are:

Spacing errors	±0.0005 inch
Tilt of surface errors	±0.001/D inch
Radii of curvature errors	±0.125 inch

Where D is the diameter of the mirror surface.

CHAPTER 1

INTRODUCTION

Automatic design techniques which utilize modern computers have made it possible to design optical systems that promise high levels of performance. One way to achieve this performance is to include aspheric surfaces of rotation in the design. Such a surface (Smith 1966), can be represented by an equation of the form

$$z = \frac{cs^2}{1+\sqrt{1-c^2s^2}} + ADs^4 + AEs^6 + AFs^8 + AGs^{10}.$$

The value of z is the coordinate along the optic axis of a point on the surface which is a distance, s, from the optic axis. The curvature of the surface at its vertex is denoted by c, and the constants AD, AE, AF and AG are the aspheric deformation coefficients. In earlier days, these were avoided because of the great computational difficulties involved in the design process. Computers have reduced these difficulties, and high performance designs with aspheric surfaces are readily attainable.

The actual performance of a fabricated system may fall short of the design values due to the cumulative effects of manufacturing errors. Presently, no automatic design program considers the sensitivity of an optical system to the degradation in performance which is caused by these errors. The great difficulty in fabricating aspheric surfaces makes it unattractive to risk large sums of money in an untried design. However, computers may still be used to estimate the performance of the constructed system. A number of computer programs exist which simply evaluate the performance of a given design. We can construct several mathematical models of the types of systems we expect to achieve in practice and use the evaluation programs to estimate their performance.

This thesis is addressed to the study of manufacturing errors in the Meinel-Shack Three-Mirror Camera. It consists of three aspheric mirror surfaces and yields a flat field. The good theoretical performance of this type of system, which is a result of using three aspheric surfaces, makes it a good system in which to study the effects of manufacturing errors. One would like to know if the design can tolerate reasonable construction errors and still approach its theoretical high performance.

A common problem with the Meinel-Shack Three-Mirror Camera is elimination of stray light or sky light. The layout of the design results in a compact system, but the resulting geometry of the system also allows a great deal of stray light to strike the image plane. This light is objectionable because it reduces the contrast of the image. Elimination of sky light is termed sky baffling, and part of this thesis is concerned with the problem of sky baffling in the Meinel-Shack Three-Mirror Camera.

The first stage of this study was to optimize the geometry, sky baffling and aspheric surfaces for a good design. Originally, a great number of systems were optimized for geometry and sky baffling. From these, two designs were selected, and the performance of both was optimized by using aspheric surfaces.

The second stage was to select the design with the best performance and study its sensitivity to manufacturing errors. The errors included here were tilts and displacements of the surfaces and changes in their spacings and curvatures. A table was made which shows the predicted resolving power of the system as a function of the magnitude of the manufacturing errors.

Since the final design is intended to be part of a design proposal, it must satisfy a number of requirements. These are:

1. 24 inch aperture
2. f-number between f/4 and f/5
3. One degree full field (edge to edge)

In addition, the system must possess as low an obscuration ratio as possible. The obscuration ratio is the ratio of the diameter of the obscuration caused by the secondary to the diameter of the aperture. Finally, the image must be accessible outside the barrel of the camera.

CHAPTER 2

NOMENCLATURE AND SIGN CONVENTION

Figure 1 illustrates a typical layout of a three-mirror system. Elements 1, 2, and 3 are the primary, secondary, and tertiary respectively. They are the only image forming elements in the design. Surface 4 is a folding flat which is inclined at an angle of 45° with respect to the optic axis. It folds the image outside of the camera barrel. The image plane is labeled as Surface 5. The secondary functions as the aperture stop of the system. A hole is punched through its center to allow a shaft to be inserted. This shaft serves as the mount for the folding flat. The secondary is mounted in a ring mount as shown in the drawing. The cylindrical tube around the tertiary serves as a sky baffle to block some of the stray light. In the figure, we see that the final image is formed inside of a tube called the image cell. This tube also serves as a sky baffle. The cup shaped housing labeled "A" is used to cover a motor which is mounted behind the secondary. The motor is connected to a shaft which rotates the folding flat. In this way the final image can be made to fall on any one of a series of detectors mounted on the camera barrel. The barrel of the camera is shown and completes

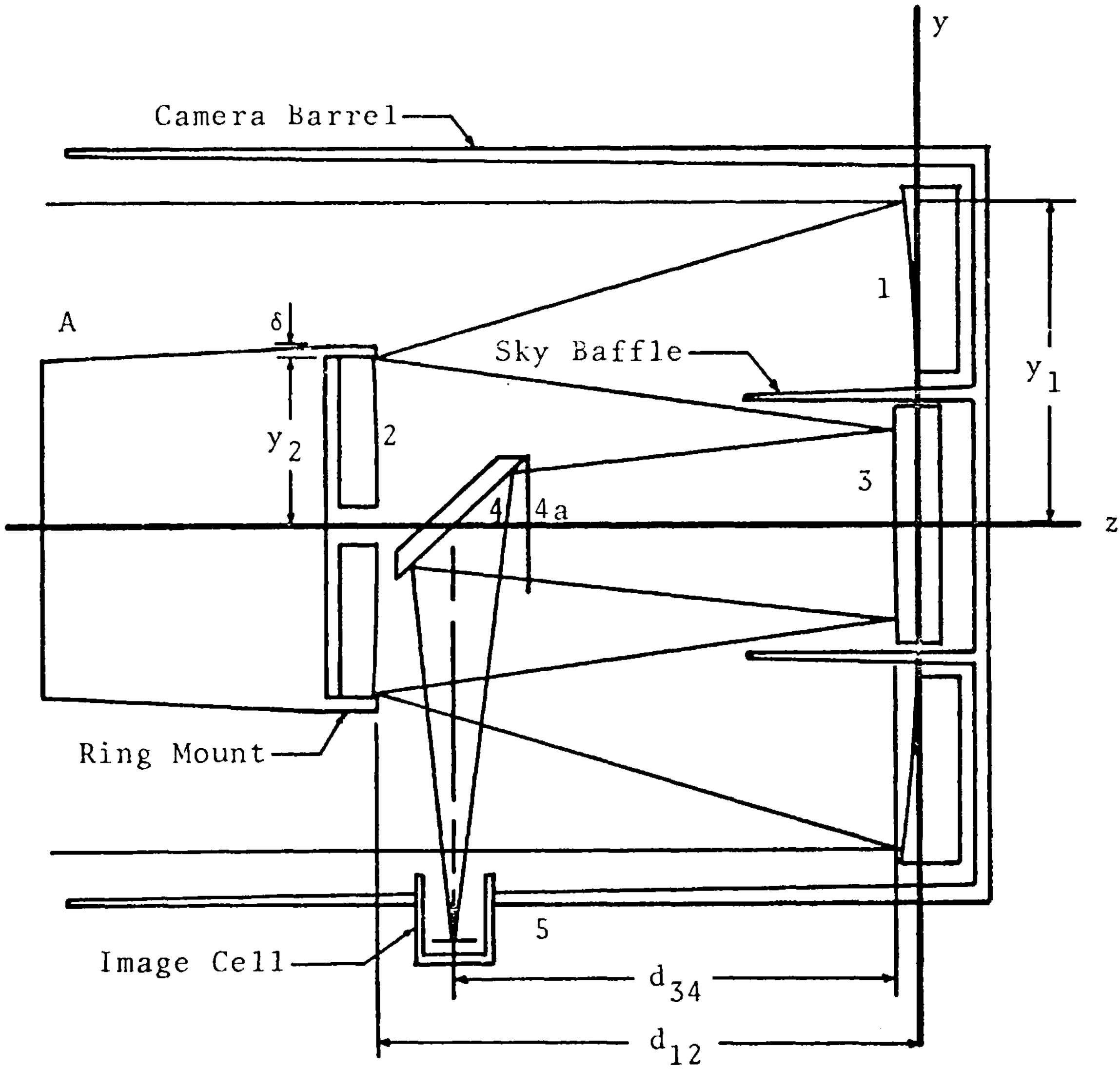

Fig. 1. Typical Layout of a Three-Mirror Camera

the layout of a typical system.

Figure 1 also illustrates the notation which will be used. The coordinate system is a right-handed cartesian coordinate system with its origin at the vertex of the primary, and the z-axis coincides with the optic axis. The plane of Figure 1 is the y-z plane. Distances measured from left to right and from bottom to top are positive. The heometric distance between any two surfaces, m and n is measured from their vertexes and is denoted by d_{mn}, with $d_{mn} = -d_{nm}$. The distance between the primary and secondary is d_{12}. The marginal ray height at any point is y, and $\bar{y}$ is the chief ray height at any point. The marginal ray height at surface m is denoted by y_m. The thickness of the ring mount for the secondary is δ. A dummy surface, labeled 4a and normal to the optic axis, is located where the upper rim ray strikes the folding flat.

The radius of curvature of a surface is measured from its vertex to the center of curvature, and is positive if the center of curvature is to the right of the surface. In the case where the primary is concave and the secondary is convex, this results in both radii of curvature being negative. The radius of curvature of the *ith* surface is denoted by R_i, and the curvature, c_i, is defined as

$$c_i = \frac{1}{R_i} .$$

The indices of refraction before and after the *ith* surface are n_i and n_i' respectively. After a reflection, the sign of n_i' is the opposite of n_i. The angles of the chief and marginal rays with respect to the optic axis are $\bar{u}$ and u respectively. To determine the sign, rotate the ray through the smallest angle which will make it parallel to the optic axis. A clockwise rotation is positive and counter-clockwise is negative.

CHAPTER 3

SATISFYING THE GEOMETRY OF THE CONSTRAINTS

In the introduction some design requirements were listed as being necessary to satisfy a design proposal. One way of arriving at a system to satisfy these requirements is to do the first order design work using $y,\bar{y}$ diagrams (Delano 1963). Readers not familiar with $y,\bar{y}$ diagrams should read Appendix A. In this chapter, we will impress each requirement, one at a time, onto a $y,\bar{y}$ diagram and eventually arrive at a limited number of designs which will satisfy the requirements listed in the introduction.

Plot of a Three-Mirror Camera

Figure 2 is a plot of a general three-mirror system on a $y,\bar{y}$ diagram. Point A, whose coordinates are $\bar{y}_1$ and y_1, locates the primary. Point B $(\bar{y}_2,y_2)$ locates the secondary on the diagram. Points D $(\bar{y}_3,y_3)$, E $(\bar{y}_4,y_4)$ and F $(\bar{y}_5,y_5)$ locate the tertiary, folding flat, and image plane respectively. Point C $(\bar{y}_c,y_c)$ represents a dummy surface which will be useful later. Since the secondary serves as the aperture stop, we have $\bar{y}_2=0$, and B lies on the y axis at all times. Now, the entrance pupil is the image of the stop in object space. In this particular case, the entrance pupil is the image formed by the primary of the

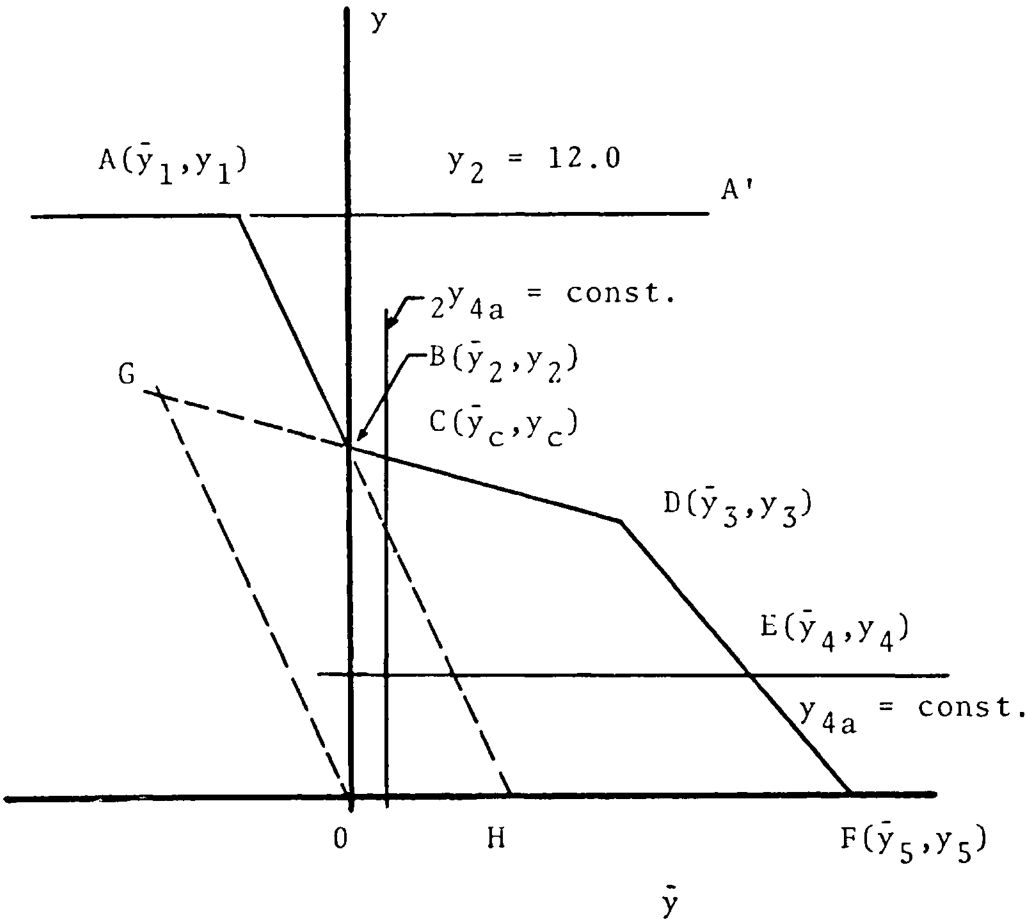

Fig. 2. Plot of a General Three-Mirror Camera

secondary. One of our requirements is for the aperture to be 24 inches in diameter. Therefore the marginal ray height at the primary, y_1, must be equal to 12.0 inches, and the primary is always located on the line $y_1 = 12.0$ (Fig. 2).

Other specifications which are given include the field angle, $\bar{u}_o$, and the f-number, F. Using these, we can find the location of the image on the $y,\bar{y}$ diagram. At the image, $y_5 = 0$, and $\bar{y}_5 = 2Fy_1\bar{u}_o$. The image point always has these coordinates.

Condition on the Diameter of the Folding Flat

In Figure 1, we see that a cone of light is reflected from the secondary toward the tertiary. However, some of the inner rays of this cone may be intercepted by the back of the folding flat. This would have the same effect as increasing the obscuration ratio of the system. We would like to find the maximum diameter of the folding flat which doesn't obscure any of the inner rays in the cone.

A ray which is parallel to the optic axis when it enters the system and just grazes the central obstruction, before striking the primary, will be called the "innermost axial ray." The obscuration ratio, ρ, can then be written as the ratio of the innermost axial ray height to the marginal ray height. That is,

$$\rho = \frac{y_1'}{y_1} . \tag{3.1}$$

Where y_1' is the height of the innermost axial ray at the primary. Now, at the primary,

$$y_1' = y_2 + \delta . \tag{3.2}$$

Since the marginal ray and innermost axial ray are initially parallel, and they both converge toward the same focal point, we have, at any point along the optic axis,

$$y' = \rho y . \tag{3.3}$$

To avoid vignetting the light which is reflected from the tertiary to the folding flat, the minor diameter of the folding flat, D_4, must satisfy the relationship

$$2(|y_4| + |\bar{y}_4|) \leq D_4 . \tag{3.4}$$

And, to avoid obstructing inner axial rays reflected from the secondary, D_4 must satisfy

$$D_4 \leq 2|{}_2y_4'| . \tag{3.5}$$

Where ${}_2y_4'$ is the innermost axial ray height at the back of surface four immediately after reflection from the secondary. Now, we combine the last three equations to get

$$|y_4| + |\bar{y}_4| \leq \rho |{}_2y_4| . \tag{3.6}$$

The Dummy Surface

So far, the fact that the folding flat is tilted has been ignored. This can be allowed for by considering a dummy reflecting surface which is normal to the optic axis and placed just before the folding flat. This is surface 4a in Figure 1. Equation 3.6 then becomes

$$\left| y_{4a} \right| + \left| \bar{y}_{4a} \right| \leq \rho \left| 2 y_{4a} \right| . \qquad (3.7)$$

Equation 3.7 will be used later to eliminate some of the possible systems which we will determine.

With a need for the dummy surface established, it is now possible to enter more data on the $y,\bar{y}$ diagram. The requirement that the image be folded outside the camera barrel establishes a minimum length for d_{45}. With this, it is possible to determine y_{4a}.

$$y_{4a} = \frac{d_{45} + d_{4a4}}{2F} \qquad (3.8)$$

For fixed values of d_{45} and d_{4a4}, y_{4a} is a constant and we can plot 3.8 on the $y,\bar{y}$ diagram. All the coordinates for the dummy surface must lie on this line.

For any system which we design, there will be a minimum distance, d_{24a}, between the secondary and the back of the dummy surface. This distance must be large enough to admit placement of the folding flat. In Chapter 5, we will choose a value for d_{24a} which is large enough to be used on a great many systems.

The optical obscuration ratio, ρ', ignores the thickness of the ring mount, and it is defined simply as

$$\rho' = \frac{y_2}{y_1} . \tag{3.9}$$

Given d_{24a} and the optical obscuration ratio, it is possible to plot all the coordinates of the location of the back of the dummy surface. On the $y,\bar{y}$ diagram in Figure 2, the distance d_{24a} is proportional to the area of triangle OBC. Then, from Appendix A,

$$d_{24a} = n_2' \frac{y_2 \; {}_2\bar{y}_{4a}}{H} . \tag{3.10}$$

Where H is the Lagrange invariant (Longhurst 1957), and, at the entrance pupil, it is given by

$$H = n_o \bar{u}_o y_o . \tag{3.11}$$

From 3.9 and 3.10, we have

$${}_2\bar{y}_{4a} = \frac{H \; d_{24a}}{\rho' y_1} , \tag{3.12}$$

and ${}_2\bar{y}_{4a}$ is a constant and, as shown in Figure 2, can be plotted on a $y,\bar{y}$ diagram.

Several things have now been established on the $y,\bar{y}$ diagram. The locations of the secondary and the image plane are known by defining four system parameters. These are the aperture, obscuration ratio, f-number, and field angle. In addition, fixing the distances d_{45}, d_{24a}, and d_{4a4} determines the loci of all possible locations for the front and back surfaces of the dummy flat. Also the locus of all primaries is established by the size of the aperture.

Curvature and Spacing of the Tertiary

Figure 1 shows that the distance from the back of the dummy surface to the tertiary must equal the distance from the tertiary to the front of the dummy surface. That is,

$$d_{4a3} = -d_{34a} \ . \tag{3.13}$$

On the $y,\bar{y}$ diagram of Figure 2, this is equivalent to requiring area OCD equal to area ODE.

$$\text{Area OCD} = 1/2 \ (y_2\bar{y}_3 - y_{22}\bar{y}_{4a}) \tag{3.14}$$

$$\text{Area ODE} = 1/2 \ (\bar{y}_5 y_3 - \bar{y}_5 y_{4a}) \tag{3.15}$$

From equations 3.14, 3.15, 3.9, 3.10 and 3.8, we have

$$y_3 = \frac{\rho'}{2\bar{u}_o F} \ \bar{y}_3 - \frac{d_{24a} - (d_{4a4} + d_{45})}{2F} \tag{3.16}$$

Equation 3.16 is the equation of a straight line which is the locus of all tertiaries which will satisfy the given system parameters.

Now, for any set of coordinates y_3 and $\bar{y}_3$, it is possible to determine ${}_2y_{4a}$ and $\bar{y}_{4a}$. From Figure 2, we see that

$$\frac{y_2 - {}_2y_{4a}}{{}_2\bar{y}_{4a}} = \frac{y_2 - y_3}{\bar{y}_3} . \tag{3.17}$$

$${}_2y_{4a} = \frac{{}_2\bar{y}_{4a}}{\bar{y}_3} (y_3 - y_2) + y_2 . \tag{3.18}$$

Also, from Figure 2,

$$\frac{y_3}{\bar{y}_5 - \bar{y}_3} = \frac{y_{4a}}{\bar{y}_5 - \bar{y}_{4a}} . \tag{3.19}$$

$$\bar{y}_{4a} = \frac{y_{4a}}{y_3} (\bar{y}_3 - \bar{y}_5) + \bar{y}_5 \tag{3.20}$$

We can now check the inequality 3.7 for any pair of coordinates y_3 and $\bar{y}_3$. If it doesn't hold, we know that the folding flat will be large enough to obscure some of the inner axial rays. We then reject those coordinates. If it does hold, we can immediately determine the distances d_{23} and d_{34a} and the curvature, c_3, of the tertiary. They are given by the equations:

$$d_{23} = n_2' \frac{y_2 \bar{y}_3}{H} \tag{3.21}$$

$$d_{34a} = n_3' \frac{y_3 \bar{y}_{4a} - y_{4a} \bar{y}_3}{H} \tag{3.22}$$

$$c_3 = \frac{1}{2d_{34a}} \frac{(y_3 - y_2)(\bar{y}_{4a} - \bar{y}_3) - (y_{4a} - y_3)(\bar{y}_3 - \bar{y}_2)}{(y_2 \bar{y}_3 - y_3 \bar{y}_2)} \tag{3.23}$$

We have arrived at a curvature for the tertiary which guarantees that the diameter of the folding flat will not be large enough to obscure any inner axial rays. This was done without knowing the powers of either the primary or the secondary.

Curvatures and Spacing of Primary and Secondary

At this point, choosing any pair of coordinates for the primary will completely specify the system; the powers of the primary and secondary and their spacing can be determined. This occurs because the coordinates of both the secondary, tertiary and image have been determined. The flat field of the Meinel-Shack Three-Mirror camera requires the Petzval sum to be zero. Introduction of this requirement into the system allows us to determine the powers of the primary and secondary.

The condition for the Petzval sum to be zero is

$$\sum_k \left(\frac{1}{n'_k} - \frac{1}{n_k}\right) c_k = 0.$$

By expanding and substituting values for n, we get

$$c_1 - c_2 + c_3 = 0. \tag{3.24}$$

To find the focal length of the primary, extend line AB (Fig. 2) until it crosses the $\bar{y}$ axis at point H. The area OAH is proportional to the focal length, f_1.

$$f_1 = n'_1 \frac{y_1 \bar{y}_H}{H}$$

$$f_1 = n'_1 \frac{y_1 y_2}{H \, m_{ab}}$$

Where m_{ab} is the slope of line AB.

Since $$c = \frac{1}{2f},$$

we have $$c_1 = - \frac{H \, m_{ab}}{2n'_1 \, y_1 y_2}. \tag{3.25}$$

From Appendix A, the focal length of the secondary is proportional to the area OBG.

$$f_2 = n_2' \frac{y_2 \bar{y}_G}{H} \tag{3.26}$$

The equation of line BD is

$$y = m_{bd} \bar{y} + y_2, \tag{3.27}$$

with

$$m_{bd} = \frac{y_3 - y_2}{\bar{y}_3} . \tag{3.28}$$

Now, y_2 is a constant and values for y_3 and $\bar{y}_3$ are known. The equation of line OG is

$$y = m_{ab} \bar{y} \tag{3.29}$$

By setting equation 3.27 equal to 3.29, we can determine the coordinates of G.

$$\bar{y}_G = \frac{y_2}{m_{ab} - m_{bd}}$$

Then, from 3.26,

$$f_2 = \frac{n_2' y_2^2}{H (m_{ab} - m_{bd})} ,$$

and

$$c_2 = \frac{H\ (m_{ab} - m_{bd})}{2n_2' y_2^{\ 2}} . \tag{3.30}$$

The condition for zero Petzval sum may now be written in terms of one variable. Place 3.30 and 3.25 into 3.24 then,

$$- \frac{H\ m_{ab}}{2n_1' y_1 y_2} - \frac{H(m_{ab} - m_{bd})}{2n_2' y_2^{\ 2}} + c_3 = 0 .$$

We solve for m_{ab} and get,

$$m_{ab} = 2 \frac{\dfrac{c_3 y_2}{H} + \dfrac{m_{bd}}{2n_2'\ y_2}}{\dfrac{1}{n_1' y_1} + \dfrac{1}{n_2'\ y_2}} . \tag{3.31}$$

All the terms on the right are known, and a value for m_{ab} can be determined. Then, equations 3.25 and 3.30 may be solved for the curvatures of the primary and secondary respectively.

The distance from the primary to the secondary is proportional to the area OAB.

Therefore,

$$d_{12} = n_1' \frac{y_2 \bar{y}_1}{H} . \tag{3.32}$$

From Figure 2, we have,

$$y_1 = y_2 + m_{ab}\bar{y}_1,$$

$$\bar{y}_1 = \frac{y_1 - y_2}{m_{ab}} = \frac{1 - \rho'}{m_{ab}} y_1,$$

$$d_{12} = \frac{y_2 y_1}{m_{ab} H}(1 - \rho').$$

By using equation 3.25,

$$d_{12} = f_1 (1 - \rho'),$$

$$d_{12} = \frac{1 - \rho'}{2c_1} . \tag{3.33}$$

We now have the focal lengths of all three aspheric mirrors, the spacings between them, and the location of the folding flat. The system parameters which must be known are:

1. Aperture
2. Field Angle
3. f-number
4. The distance between the back of the dummy surface, and the secondary mirror

5. The distance between the dummy surface and the image

6. Optical Obscuration Ratio

Parameters 1, 2 and 3 are dictated by the use for which the system is designed. Reasonable values for parameters 4 and 5 may be chosen based on the need to have the image folded outside of the camera barrel. One through five are used in equation 3.16 to arrive at the locus of all tertiaries, if we have a value for ρ'. Then we can use equations 3.8, 3.18 and 3.20 to solve for y_{4a}, ${}_2y_{4a}$ and $\bar{y}_{4a}$ respectively. By substituting these values into the inequality 3.7 we can determine if a system is possible with the coordinates y_3 and $\bar{y}_3$.

CHAPTER 4

SKY BAFFLING

The geometry of a three-mirror camera (Fig. 1) allows a great deal of stray light to reach the image plane unless precautions are taken. This light produces a background light level in the image plane which results in reduced contrast in the image. Further degradation in the image will result if the background level is not constant over the image plane. This chapter considers the possible paths for stray light and ways to eliminate them.

Possible Stray Light Paths

There are three possible paths for sky light to reach the image field. One is for off-axis light to be reflected from the primary, directly to the folding flat and then to the image field. This is shown by paths A and D in Figure 3. Another path is shown by B in Figure 3. Here light strikes the tertiary without striking the primary or secondary and then is reflected from the flat to the image field. The third path is a result of requiring the image field to be outside the barrel. Light enters the open end of the barrel and directly strikes the image field as shown by path C.

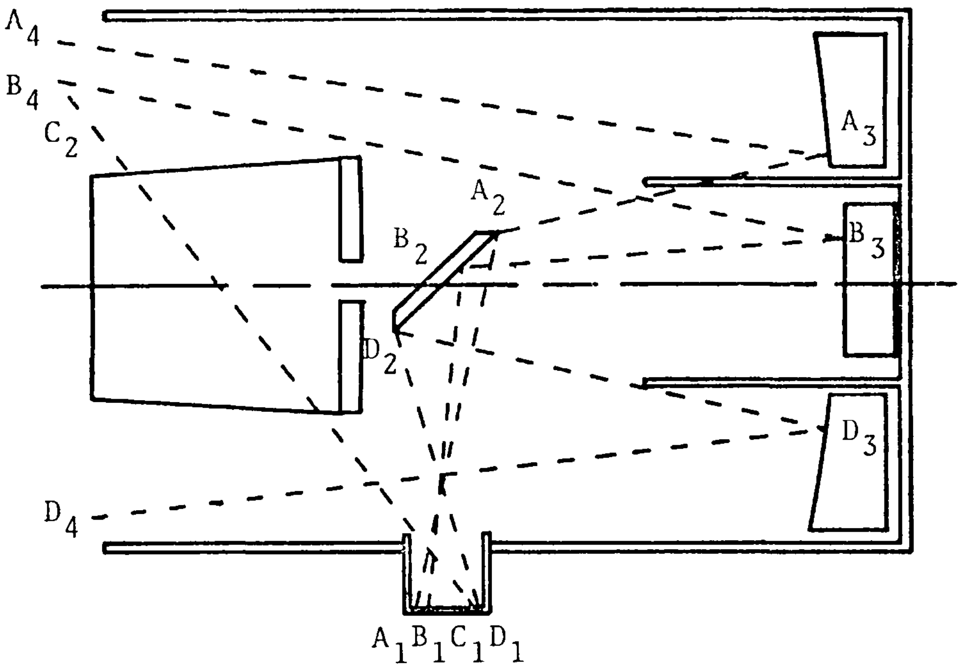

Fig. 3. All Possible Stray Light Paths

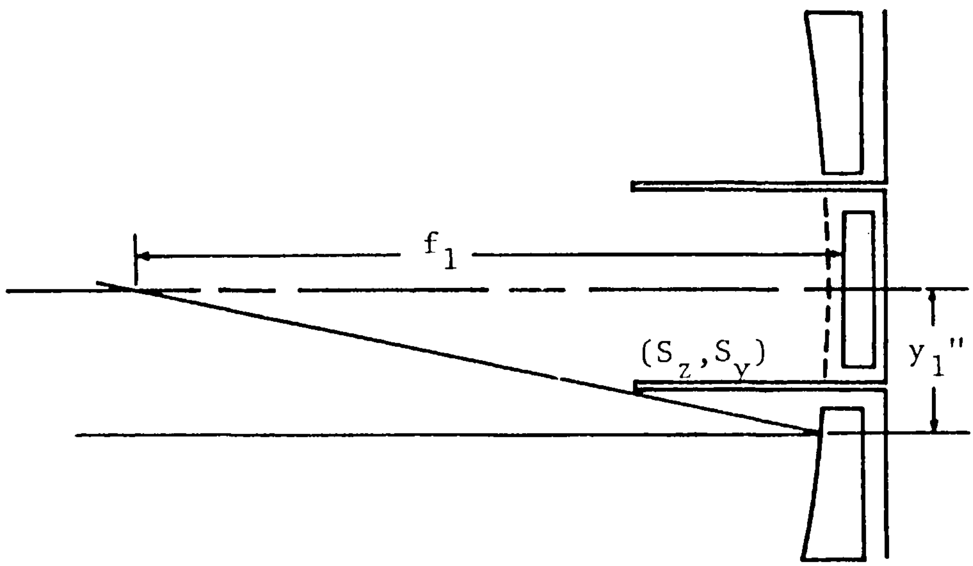

Fig. 4. Calculation of Effective Obscuration Ratio, ρ_e

Elimination of Paths A and D

Figure 3 illustrates the method of eliminating paths A and D. A cylindrical baffle is wrapped around the tertiary and is inserted far enough into the barrel to intercept these paths. The paths illustrated were actually drawn from the edges of the image field to opposite edges of the folding flat and then reflected to the primary. These are extreme paths in the sense that any other path from the image field to the flat will lie inside the cone $A_2A_3D_2D_3$ after reflection. Examination of Figure 3 shows that an extension of the baffle to intercept path D will automatically eliminate path A. Reduction of the diameter of the baffle and further extension of it will reduce the amount of stray light using path B. However, a lower rim ray of the main optical path between the secondary and tertiary might then be vignetted. Accordingly, we want the end of the baffle to be placed at the point where path D and the lower rim ray intersect.

In Figure 3, D_2 is the point where the lower rim ray between the tertiary and final image intersects the folding flat. This point determines the size of the flat and the path for the extreme ray of stray light.

The equation for the lower rim ray between the secondary and tertiary is easy to determine. The tertiary is located at $z = d_{13}$ and the lower rim ray strikes it at a height, h_3.

$$-h_3 = |y_3| + |\bar{y}_3| \tag{4.1}$$

The secondary is located at $z = d_{12}$, and the lower rim ray strikes it at a height, h_2.

$$h_2 = -|y_2| \tag{4.2}$$

These locate two points, and we use the two point form of the equation for a straight line.

$$y - h_2 = \left(\frac{h_2 - h_3}{d_{12} - d_{13}}\right)(z - d_{12})$$

$$y = \left(\frac{|y_3| + |y_3| - |y_2|}{d_{12} - d_{13}}\right)(z - d_{12}) - |y_2| \tag{4.3}$$

The equation for the extreme ray of stray light between the flat and primary is more difficult. First, we must determine the point D_2. Imagine the folding flat is removed, and the final image is formed behind the secondary. Two known points on the lower rim ray are one on the tertiary, and one on the edge of the image field. For the tertiary, the coordinates are:

$$z = d_{13}$$

$$-y = -h_3 = |y_3| + |\bar{y}_3|$$

For the image plane, the coordinates are:

$$z = d_{15}$$

$$y = h_5 = -\left|\bar{y}_5\right|$$

Again we use the two point form for the equation of a straight line.

$$y + \left|\bar{y}_5\right| = \frac{h_5 - h_3}{d_{15} - d_{13}} (z - d_{15})$$

$$y = \frac{\left|y_3\right| + \left|\bar{y}_3\right| - \left|\bar{y}_5\right|}{d_{15} - d_{13}} (z - d_{15}) - \left|\bar{y}_5\right| \qquad (4.4)$$

with

$$d_{15} - d_{13} = d_{34} + d_{45}$$

The equation for the folding flat is

$$y = z - d_{14}, \qquad (4.5)$$

with

$$d_{14} = d_{13} + d_{34}.$$

By solving equations 4.4 and 4.5 for z and y, we have the coordinates of point D_2.

These coordinates of D_2 give us one point on the extreme sky ray. The slope of this ray, m, can be shown to be

$$m = \frac{d_{12} + d_{24} + \bar{y}_5 - D_{2z}}{-d_{45} \quad -D_{2y}} , \tag{4.6}$$

where D_{2z} is the z coordinate of D_2. The equation of the sky ray is then

$$y - D_{2y} = m\,(z - D_{2z}) \tag{4.7}$$

Equating equations 4.3 and 4.7 then allows us to determine the z and y coordinates of the end of the cylindrical baffle.

Now, it may happen that the baffle may intercept some of the inner axial rays which were reflected from the primary. This would effectively increase the obscuration ratio. We would like to know where an inner axial ray must strike the primary in order to clear the end of the baffle. Figure 4 is a sketch of the primary with focal length f_1. Let S_z and S_y be the coordinates of the end of the baffle, and y_1'' be the height of the inner axial ray which grazes the end of the baffle. From the figure,

$$\frac{y_1''}{f_1} = \frac{S_y}{f_1 - S_z} .$$

$$y_1'' = \frac{S_y}{f_1 - S_z}\, f_1 \tag{4.8}$$

We can compare this value of y_1'' with the value of y_1' in equation 3.3. If y_1'' is greater than y_1', then we have an effective obscuration ratio, ρ_e, given by

$$\rho_e = \frac{y_1''}{y_1} \tag{4.9}$$

The effective obscuration ratio will be discussed more fully in Chapter 5.

Elimination of Path C

Path C (Fig. 3) can be eliminated in two ways. One is extension of the tube length, and the other is by increasing the depth of the image cell. The housing around the mount for the secondary also blocks some of the light which uses this path. The maximum depth of the image cell is determined by the distance d_{45} and the requirement that the cell obstructs none of the image forming light which enters the barrel. This leaves only the barrel length to be determined.

As one looks into the image cell (Fig. 5-d) from the sky, he observes a "cat's eye" formed by the edges of the image field and the upper end of the image cell. There is a set of rays which grazes the upper rim, passes through the optic axis, and strikes the edge of the image field. The "cat's eye" diminishes to a point when viewed along one of these rays. The barrel and central obscuration will intercept some of these rays, and, for the minimum barrel length, all but one ray will be intercepted. We want to find the z coordinate of the intersection of this ray with the camera barrel.

Figure 5 demonstrates a graphical method of determining the minimum tube length. Section d is a magnified view of the image cell. The distances labeled y_d and d are the radius and depth of the cell respectively. To find the point where the ray crosses the optic axis, we draw a ray from the edge of the well to the edge of the field. Point G is the intersection point. Label the distance from the image plane to the intersection L. We next transfer L, scaled down of course, to section a. In Figure 5-a, the inner circle is an end on view of the central obscuration and the outer circle is the camera barrel. Draw a line from point G, tangent to the central obscuration, and intersecting the barrel at point B. This line establishes two points, the x and y coordinates of the intersections of the ray with the end of the barrel and the intersection with the open end of the image cell. These intersections are points B and E respectively. In Figure 5-b, the small circle is an end on view of the image cell. Transfer the x coordinate of point E from section a to the small circle in section b (Fig. 5). The center of the circle is the xz projection of point G. Draw a straight

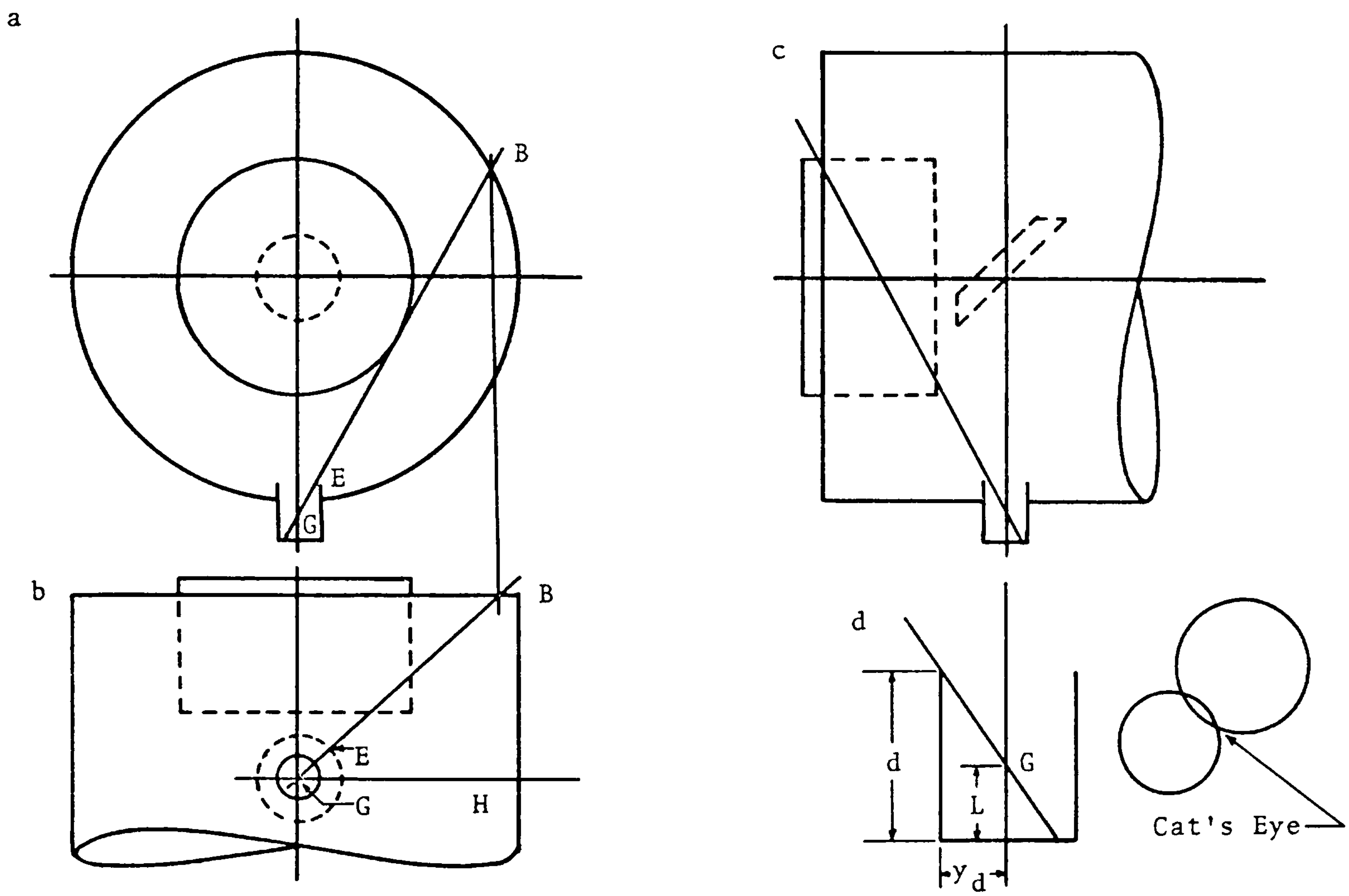

Fig. 5. Determination of Additional Tube Length

line from point G through E, and extend it upward. Now drop a line vertically downward from B in section a (Fig. 5). The intersection of these two lines establishes the end of the camera barrel. The distance BH, in section b, is the extension beyond the folding flat which is needed for eliminating stray light which falls directly on the image field. Chapter 5 sketches a numerical solution for a particular system. The steps followed, however, are the same as above.

CHAPTER 5

SELECTION OF THE FINAL SYSTEM AND ELIMINATION OF STRAY LIGHT

In Chapter 3, equations were derived which describe a set of three-mirror cameras as functions of several input parameters. These parameters were:

1. Aperture
2. Field angle
3. f-number
4. The distance between the back of a dummy surface and the secondary.
5. The distance between the dummy surface and the image.
6. Obscuration ratio

Chapter 4 considered the problems of sky baffling for the systems. The effective obscuration ratio was introduced, and a graphical solution to the tube length was outlined. This chapter will describe the use of the equations in Chapter 3 to find a suitable system and will include a numerical solution to the minimum tube length for that system.

Selection of Values for d_{24a}, d_{24}, d_{4a5} and d_{45}

The first three parameters listed are set by the requirements of the system. Now, we must decide on values for the last three. With the folding flat in place, we want the final image to lie outside the camera barrel. Also, it is desirable to have the image cell outside the incident, image-forming light. In Figure 6, this requires the entrance to be below the lower rim ray from an object point below the axis. The lower rim ray near point A will be some distance below the marginal ray. A good guess for this distance is one inch. This requires the entrance to the image cell to be thirteen inches from the vertex of the folding flat. In order to provide some sky baffling, the image cell must have some length. Let us use three inches. Therefore, the final image will be a total of sixteen inches from the vertex of the folding flat. The distance between the secondary and folding flat, d_{24}, was set at three inches. This value was found to be satisfactory when used in a system which was proposed earlier but is not included in this report. To allow for tilting of the flat, the dummy surface was placed 2.4 inches in front of the flat. This makes the distance between the secondary and dummy surface, d_{24a}, equal to 5.4 inches, and the distance between the dummy surface and image plane, d_{4a5}, equal to 18.4 inches. These two distances will insure that the

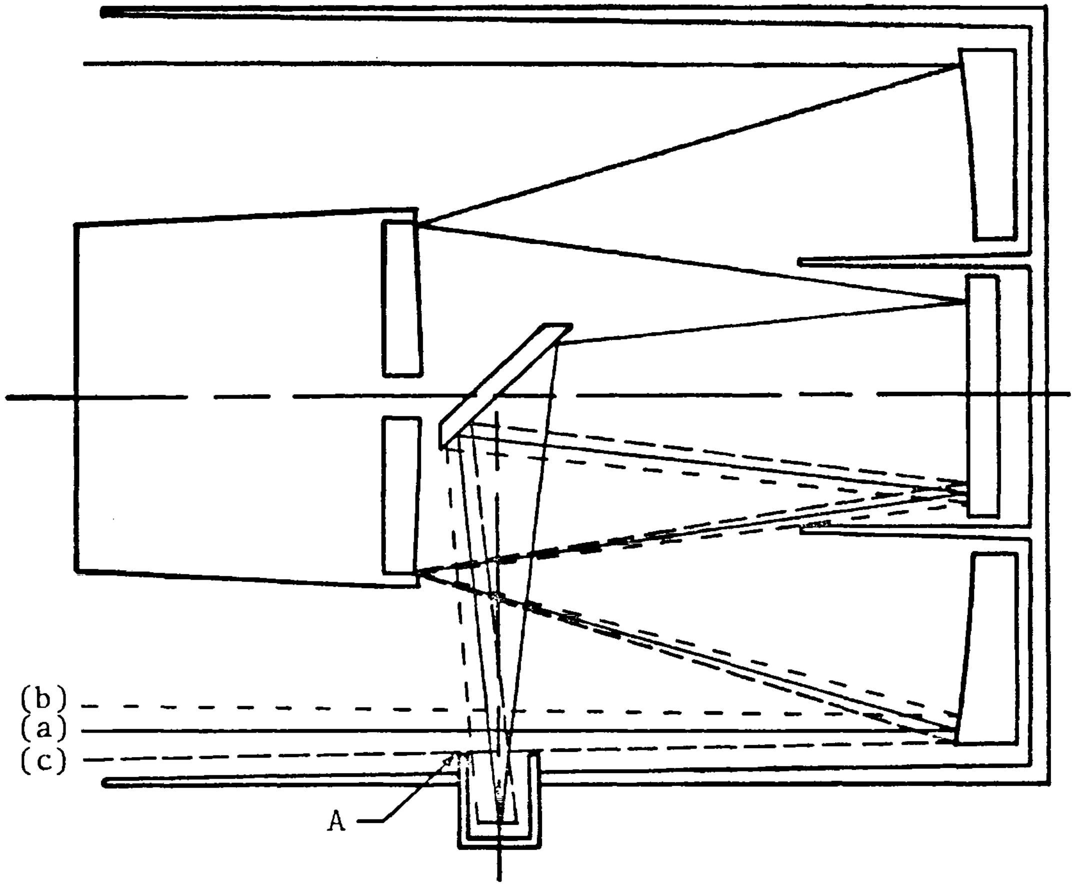

Fig. 6. Paths of: (a) Marginal Ray and Lower Rim Rays (b) and (c)

The lower rim ray (b) comes from an object point above the optic axis and the lower rim ray (c) from an object point below the optic axis.

image plane lies outside the camera barrel and that there is sufficient clearance between the secondary and folding flat.

Selection of Obscuration Ratio

A value for the obscuration ratio, ρ, must also be picked. Figure 7 shows the radial energy distributions of the image of a point source for three aberration free systems with annular apertures. The only difference between the three systems is their obscuration ratios. Here we see that as ρ is increased, energy is redistributed from the core of the image to the outer rings. For this reason, we want to pick a final design which has as low an obscuration ratio as possible.

To find this system, we have no choice but to use a process of elimination. We pick any value for ρ and then use equation 3.16 to find the locus of all tertiaries. We then take a few points on this line and see if the inequality 3.7 holds. This is done by using equations 3.8, 3.20 and 3.18 to solve for y_{4a}, $\bar{y}_{4a}$ and ${}_2y_{4a}$ respectively. If 3.7 doesn't hold for any point on the line, then we must try a larger value for ρ and continue doing this until we find 3.7 holds. With this, we can use the equations in Chapter 3 to solve for the rest of the system. In this way, we can determine the lowest possible value of ρ.

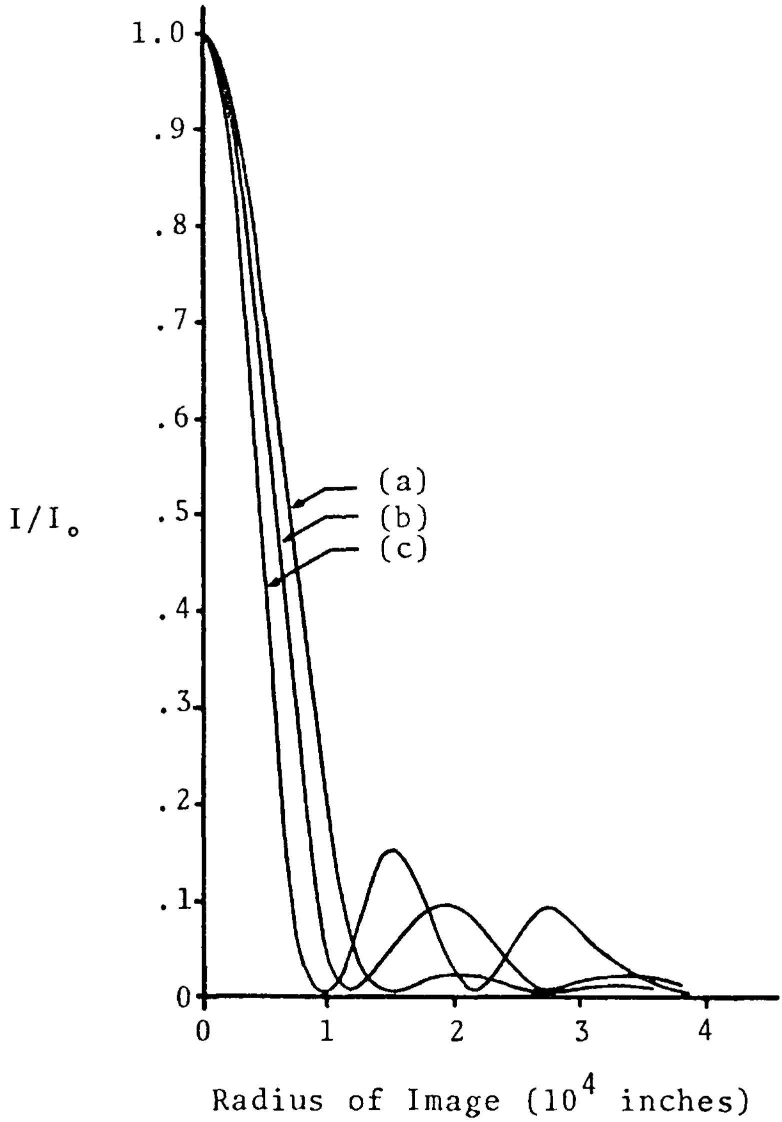

Fig. 7. Comparison of Radial Intensity Distributions for Three Aberration Free Systems with Different Obscuration Ratios

Plots are normalized intensity curves for Fraunhoffer patterns of annular apertures with (a)ρ = 0.0, (b)ρ = 0.5, (c)$\rho \rightarrow$ 1.0.

The above process is tedious indeed. To save drudgery, a computer program was written in Fortran IV to do it automatically. The parameters listed on page 33 were entered as input and the program generated many complete systems. The maximum value of $\bar{y}_3$ which was used as one such that

$$|y_3| + |\bar{y}_3| = |y_2| .$$

The value of y_3 was obtained from equation 3.16. It was felt if

$$|y_3| + |\bar{y}_3| > |y_2| ,$$

then the stray light using path B in Figure 3 would be too great. The lowest value of $\bar{y}_3$ used was for the case where

$$\bar{y}_3 = 2\bar{y}_{4a} .$$

Because it is at this point that

$$d_{4a3} = 0 .$$

The resulting interval was divided into thirty equal increments in $\bar{y}_3$ and corresponding values of y_3 were determined. This gave us thirty points along the locus of tertiaries. Each point was tested as outlined in the preceding paragraph, and complete systems determined for all points which passed the test. Several runs were made using many parameters which satisfied the requirements.

Simply choosing a system with the lowest obscuration ratio may not be the whole case. In Chapter 4, we found an effective obscuration ratio, ρ_e, which was caused by the sky baffling requirement. If ρ_e is greater than ρ, then we should look for another system which may have a greater value of ρ but a lower ρ_e. A routine was placed in the program which computed the length and diameter of the sky baffle and the corresponding value of ρ_e for every system which was determined. With this information, we can find the most desirable system in terms of the obscuration ratio.

Appendix B is a sample of the output. The focal lengths and spacings of all the mirrors are listed under the appropriate columns. XSKY and YSKY are the x and y coordinates respectively of the end of the cylindrical baffle. REQOB is equivalent to y_1'' of Chapter 4.

Selection of the Final Design

Nine runs were made with the program. Three values of δ were used with each of three values of y_2. In the sample output,

$$y_2 = 6.5 \text{ in and } \delta = 0.25 \text{ in.}$$

This gives a value for ρ of

$$\rho = 0.5625$$

In each of the runs, it was possible to find a minimum value of REQOB. This corresponds to a minimum effective obscuration ratio, $\rho_{e\ min}$, given by

$$\rho_{e\ min} = \frac{REQOB_{min}}{y_1},$$

Figure 8 is a plot of $\rho_{e\ min}$ as a function of the obscuration ratio, ρ. The three curves represent three different values of δ. The crosses locate the points which were actually computed. The dashed line represents $\rho = \rho_{e\ min}$. For points to the left of the line,

$$\rho_{e\ min} > \rho,$$

and for those to the right of the dashed line,

$$\rho > \rho_{e\ min}.$$

For any system, we must use the larger of ρ or $\rho_{e\ min}$ as the diffracting obscuration ratio, ρ_d, when computing the MTF. The diffracting obscuration is the one which has the largest projection in the pupil. Hence, we seek the system which has the smallest value of ρ_d. In Figure 8, this is point A. However, this was achieved with $\delta = 0.0$. To allow for the mounting of the secondary and beveling of the edge, δ, must be at least 0.25 inches. This leads to point B where

$$\rho_d = 0.5625.$$

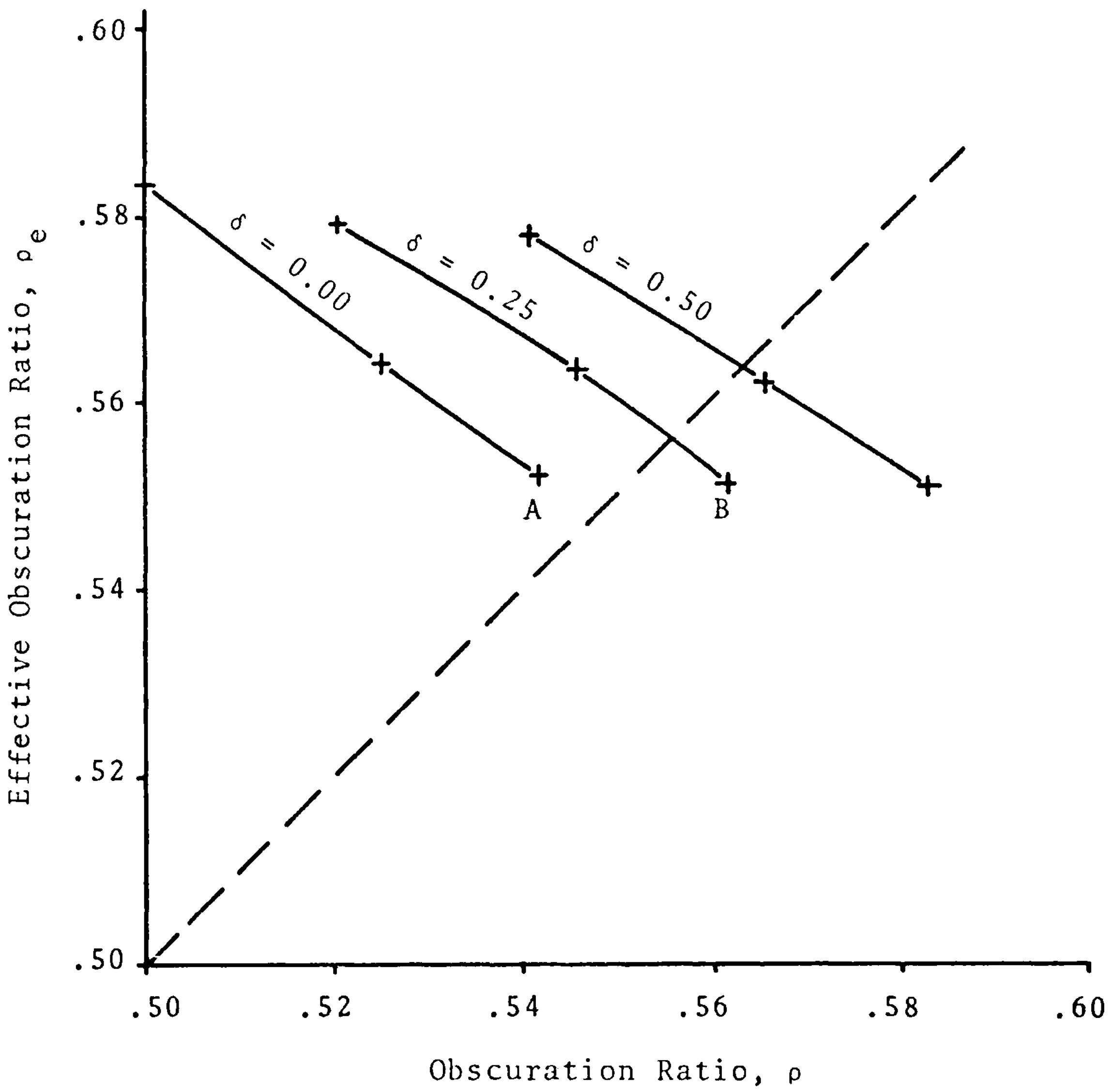

Fig. 8. Selection of Minimum Obscuration

Point B represents the design marked B in the sample output.

In the sample output, REQOB is the radius of the obscuration, in the pupil, which is caused by sky baffling. For designs B and C in the output, we see that REQOB is less than the radius of the obscuration, $y_2 + \delta$, which is caused by the secondary. Hence, the secondary causes the diffracting obscuration for these systems. For this reason, either system will be satisfactory as the one with smallest diffracting obscuration ratio. Design C was chosen because it had slower surfaces and a shorter overall length.

The primary of design C is about f/2. It was feared that this would make the design difficult to optimize. For this reason, another design called D, with slower surfaces but a larger obscuration ratio, was also selected. Figures 9 and 10 are $y, \bar{y}$ plots of designs C and D respectively.

The two systems were then optimized by varying the aspheric deformation coefficients. The actual work was performed by Gary Wilkerson at the Optical Sciences Center of The University of Arizona. He used an automatic design program on a CDC 6400 computer. The name of the program was ACCOS, and it was prepared by Gordon Spencer. Mr. Wilkerson had little trouble in achieving diffraction limited performance with the fast mirror system, but, surprisingly, the slow mirror system gave considerable trouble.

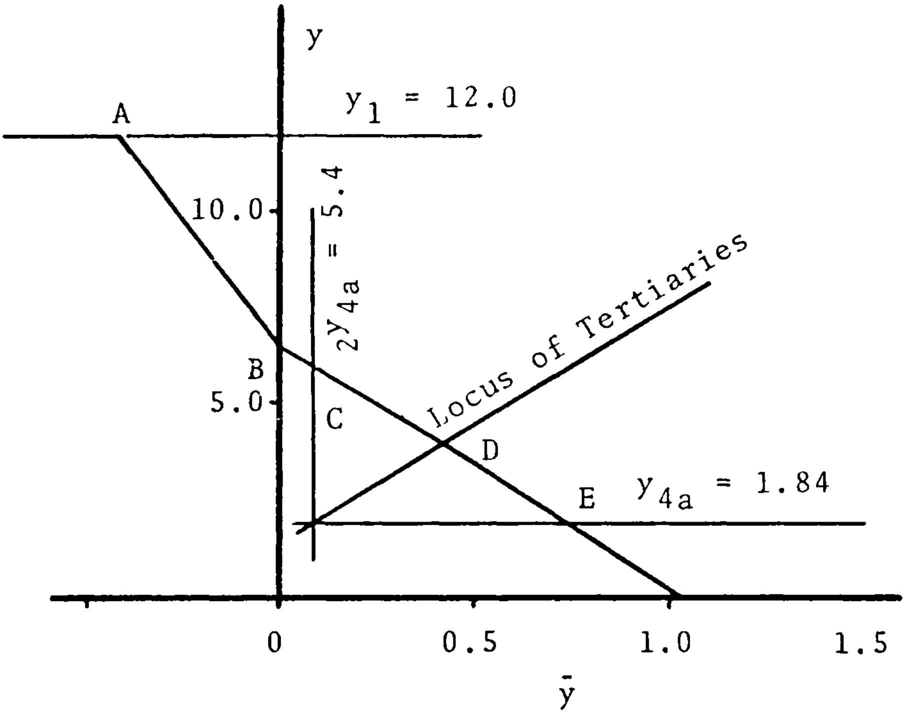

Fig. 9. $y,\bar{y}$ Diagram of Design C

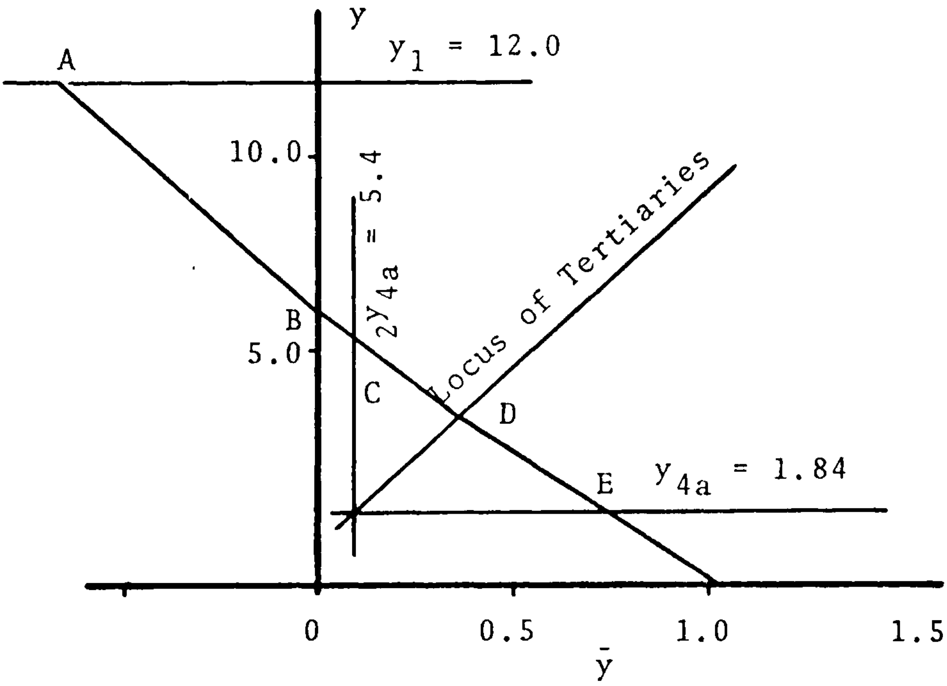

Fig. 10. $y,\bar{y}$ Diagram of Design D

It never did get to a point where it was definitely a diffraction limited system. The final systems are described in Table I. This table lists powers, spacings, and aspheric coefficients of all the surfaces. Figures 18 through 22 compare the MTFs of the two designs.

The advantages of the fast mirror design, which included a lower obscuration ratio, better performance and shorter length, led to its selection as the final design to be used in this report.

Calculation of Barrel Length

Now that the final system has been selected, we need to consider the sky baffling. Part of this was determined when ρ_e was calculated. Here it was necessary to calculate the diameter and length of the cylindrical baffle around the tertiary. All we need now is the distance the camera barrel extends beyond the folding flat. Chapter 4 contained a graphical solution to this procedure, but here we will use algebraic equations to determine the distances. It may be necessary to refer to page 29 to get an overview of the procedure.

Imagine a right-handed rectangular coordinate system with its origin at the vertex of the folding flat (Fig. 5). The ray EB is the one which was sought in Chapter 4. Point B is the intersection of the ray which closes the "cat's eye" with the end of the barrel. Now,

TABLE I

Parameters of Designs C and D

Fast Mirror System

	Curvature (in^{-1})	Spacing (in)
Primary	-0.0090284364	
		-25.382763
Secondary	-0.0088969513	
		+25.867802
Tertiary	+0.0001314351	
		-22.867802
Flat	0.000	
		+16.000
Image	0.000	

Aspheric Coefficients

	Primary	Secondary	Tertiary
AD	$+2.3345630 \times 10^{-07}$	$+2.6588390 \times 10^{-06}$	$+2.7367840 \times 10^{-06}$
AE	$+1.3720399 \times 10^{-11}$	$-1.2449869 \times 10^{-09}$	$-8.9620556 \times 10^{-10}$
AF	$-1.4896806 \times 10^{-14}$	$-2.1649256 \times 10^{-12}$	$-4.4552829 \times 10^{-11}$
AG	$+7.0987927 \times 10^{-17}$	$+4.2466697 \times 10^{-14}$	$+1.6881541 \times 10^{-12}$

TABLE I (Continued)

Fast Mirror System

f-Number =	5.000
Aperture =	24.000 in
Focal Length =	120.000 in
Field of View =	1.00 deg
Format Diameter =	1.047 in
Diameter of Stop =	13.000 in
Diameter of Obscuration =	13.500 in
Effective Obscuration Ratio =	0.5625
Diameter of Sky Baffle =	10.622 in
Length of Sky Baffle =	11.389 in

TABLE I (Continued)

Slow Mirror System

	Curvature (in^{-1})	Spacing (in)
Primary	-0.006465982	
		-38.66388
Secondary	-0.002226496	
		+20.57202
Tertiary	+0.004239487	
		-17.57202
Flat	0.000	
		+16.000
Image	0.000	

Aspheric Coefficients

	Primary	Secondary	Tertiary
AD	$+1.2268850\times10^{-07}$	$+2.0896200\times10^{-06}$	$+4.6076960\times10^{-06}$
AE	$+3.2892450\times10^{-12}$	-1.5361721×10^{-09}	-6.2905046×10^{-09}
AF	$+2.1208083\times10^{-14}$	$+1.0850102\times10^{-11}$	$+4.3487512\times10^{-10}$
AG	$+1.1249851\times10^{-18}$	-5.4902826×10^{-14}	-1.2807366×10^{-11}

TABLE I (Continued)

Slow Mirror System

f-Number	=	5.000	
Aperture	=	24.000	in
Focal Length	=	120.000	
Field of View	=	1.00	deg
Format Diameter	=	1.047	in
Diameter of Stop	=	12.000	in
Diameter of Obscuration	=	14.400	in
Effective Obscuration Ratio	=	0.60	
Diameter of Sky Baffle	=	9.4	in
Length of Sky Baffle	=	26.8	in

our goal is to find the z coordinate of point B. The value of this coordinate is the additional barrel length beyond the folding flat which is required.

Let us first find the x coordinate of B in the xy plane. The equation of line EB in this plane is

$$y = (\mathrm{CTN}\ \theta)x + (d_{45} + d')$$

$$= \frac{+\sqrt{(d_{45} + d')^2 - y_o^2}}{y_o}\, x + (d_{45} + d'). \tag{5.1}$$

Where

$$r_o = \text{radius of the central obscuration}$$

$$d_{45} = -16.0 \text{ inches},$$

since ρ is greater than ρ_e, we set

$$r_o = \rho\ y_1.$$

From Table I,

$$\rho = 0.5625$$

$$r_o = (0.5625)(12.0 \text{ in}) = 6.75 \text{ in}.$$

From Figure 5, section d, we have

$$d' = \left(\frac{L}{y_d + \bar{y}_5}\right) \bar{y}_5 \tag{5.2}$$

with y_d equal to one half the diameter of the image cell and L equal to its length. Now, we want the entrance of the image cell to be outside the converging cone of image forming light which is incident on the primary. That is,

$$L = h_a - d_{45}.$$

Where h_a is the height of the incident lower rim ray at point A in Figure 6. ACCOS was used to trace several real rim rays. Here we found that

$$h_a = -12.4622 \text{ in.}$$

Then

$$L = -12.5 + 16.0.$$

$$L = 3.5 \text{ in.}$$

To avoid vignetting, y_d should be greater than the diameter of the converging cone of light at the entrance to the image cell. That is,

$$y_a \geq h'_a \ ,$$

where h'_a is the distance from the optic axis of a rim ray at the entrance to the image cell. From the real ray trace by ACCOS,

$$h'_a = 1.337 \text{ in.}$$

Then

$$d' = \left(\frac{3.5}{1.34 + 1.04715}\right) 1.04715 = 1.535 \text{ in.}$$

Placing r_o, d_{45} and d' in equation 5.1 gives

$$y = 1.913x - 14.465 \tag{5.3}$$

as the equation of the xy projection of the desired ray. The equation of the end of the barrel in the xy plane is

$$x^2 + y^2 = r_t^{\,2}. \tag{5.4}$$

r_t = one half the diameter of the camera barrel

$$r_t = 13.25 \text{ inches}$$

The value of r_t was chosen to avoid vignetting rim rays for barrel lengths of 100 inches or less. Solving equations 5.3 and 5.4 for x results in the x coordinate of point B.

$$B_x = 11.234 \text{ in.}$$

We now wish to find the z coordinate of point E. The x coordinate of E is found by setting

$$y = d_{45} + L \tag{5.5}$$

into equation 5.3.

$$-16.0 + 3.5 = 1.913x - 14.465.$$

$$E_x = 1.027 \text{ in.}$$

Point E also lies on the small circle in section b of Figure 5. The circle is given by

$$x^2 + z^2 = y_d^{\,2}. \tag{5.6}$$

From which,

$$z = \sqrt{y_d^{\,2} - x^2}$$

$$z = \sqrt{1.7956 - 1.0551}$$

$$E_z = 0.8607 \text{ in.}$$

The x-z projection of line AB is given by

$$z = \frac{E_z}{E_x} x \, .$$

Therefore,

$$z = 0.8381x. \qquad (5.7)$$

The z coordinate of point B is found by setting $x = B_x$ in equation 5.7.

$$z = (0.8381)(11.234)$$

$$B_z = 9.415 \text{ in.}$$

That is, the end of the camera barrel must extend at least 9.5 inches beyond the vertex of the folding flat.

Stray Light Reflected From the Tertiary

We must still consider the stray light which enters by path B in Figure 3. Figure 11 is a drawing of only the secondary, tertiary and cylindrical baffle of the system. The stray light path touches the edge of the ring mount, passes just inside the cylindrical baffle and is reflected

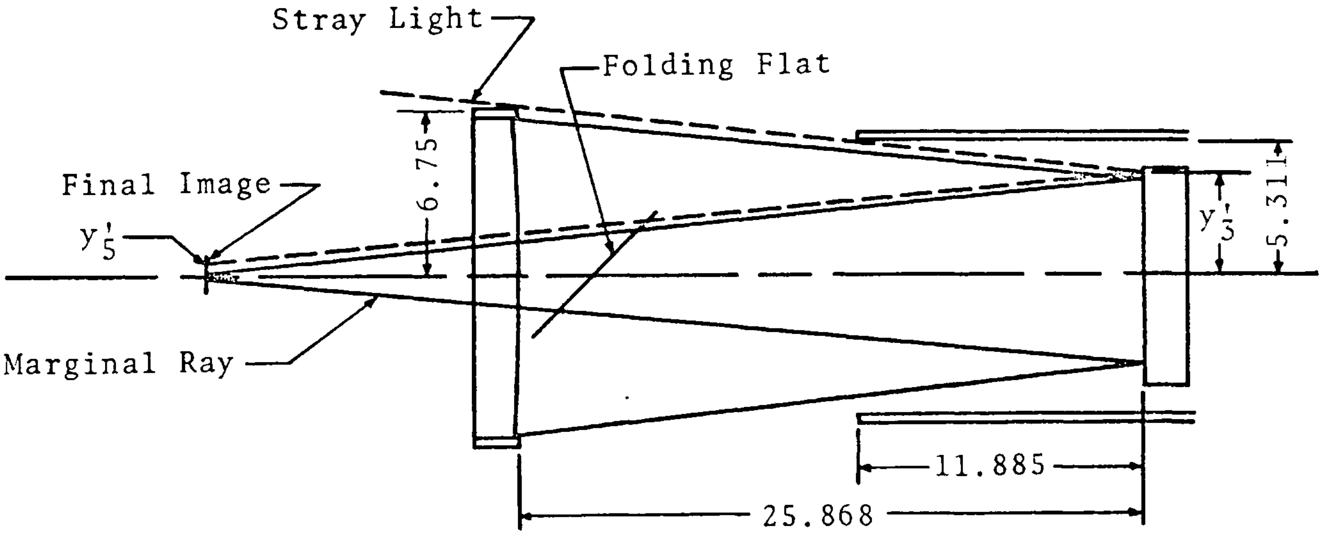

Fig. 11. Elimination of Stray Light Reflected from Tertiary

from the tertiary to the image plane. Let y_3' and y_5' be the heights where this ray intersects the tertiary and image plane respectively. From Figure 10,

$$\frac{6.75 - y_3'}{25.868} = \frac{5.311 - y_3'}{11.885} \tag{5.8}$$

$$y_3' = 4.1304 \text{ in.}$$

The stray light ray is incident upon the tertiary at an angle u_3 with respect to the optic axis.

$$u_3 = -\frac{6.75 - 4.1304}{25.868} = -0.099335.$$

We apply the refraction equation (Smith 1966) to find the angle after reflection, u_3'.

$$n_3' \, u_3' = n_3 \, u_3 - y_3' \, (n_3' - n_3) c_3 \tag{5.9}$$

$$n_3' \, u_3' = -0.098249.$$

The transfer equation (Smith 1966) gives the height that the ray strikes the image plane

$$y_5' = y_3' + \left(\frac{d_{35}}{n_3'}\right)(n_3' \, u_3') \tag{5.10}$$

$$y_5' = +0.31167 \text{ in.}$$

Since the image field is 1.04715 inches in height, we see that the stray light is within the field of the camera.

To prevent stray light from using this path, we may again increase the size of the central obscuration. Doing this will cause the stray light ray (Fig. 11) to pivot around the end of the cylindrical sky baffle. The incident angle of this ray, u_3, will then be given by

$$u_3 = - \frac{5.311-y_3'}{11.885} \tag{5.11}$$

After reflection, the angle is given by equation 5.9 with u_3 given by 5.11. Now, we want the stray light to strike the image plane at a height y_5' with

$$y_5' = -\bar{y}_5 .$$

From 5.10,

$$-\bar{y}_5 = y_3' + \left(\frac{d_{35}}{n_3'}\right)\left[-n_3 \frac{5.311-y_3'}{11.885} - y_3' (n_3' - n_3)c_3\right].$$

$$-1.04715 = y_3' + \left(\frac{-38.868}{-1}\right)\left(- \frac{5.311-y_3'}{11.885} + 0.0002629702\ y_3'\right)$$

$$y_3' = 3.8134 \text{ in.} \tag{5.12}$$

From Figure 11, the height, h, that this incident stray light ray passes the obscuration of the secondary is given by

$$h = y_3' + 25.868 \left(\frac{5.311-y_3'}{11.885}\right). \tag{5.13}$$

Substitution of 5.12 gives

$$h = 7.0728 \text{ in.} \tag{5.14}$$

Therefore, the diameter of the central obscuration must be increased to 14.146 inches if all the stray light is to be eliminated. In this case, the obscuration ratio is increased to 0.59.

Figure 12 is a drawing of the final system, with all dimensions included. Two sizes of central obscuration are shown. The one drawn with solid lines prevents stray light from using paths A and D. The other, drawn with dashed lines, prevents light from using path B as well as paths A and D. With the larger obscuration, the system is entirely free of stray light.

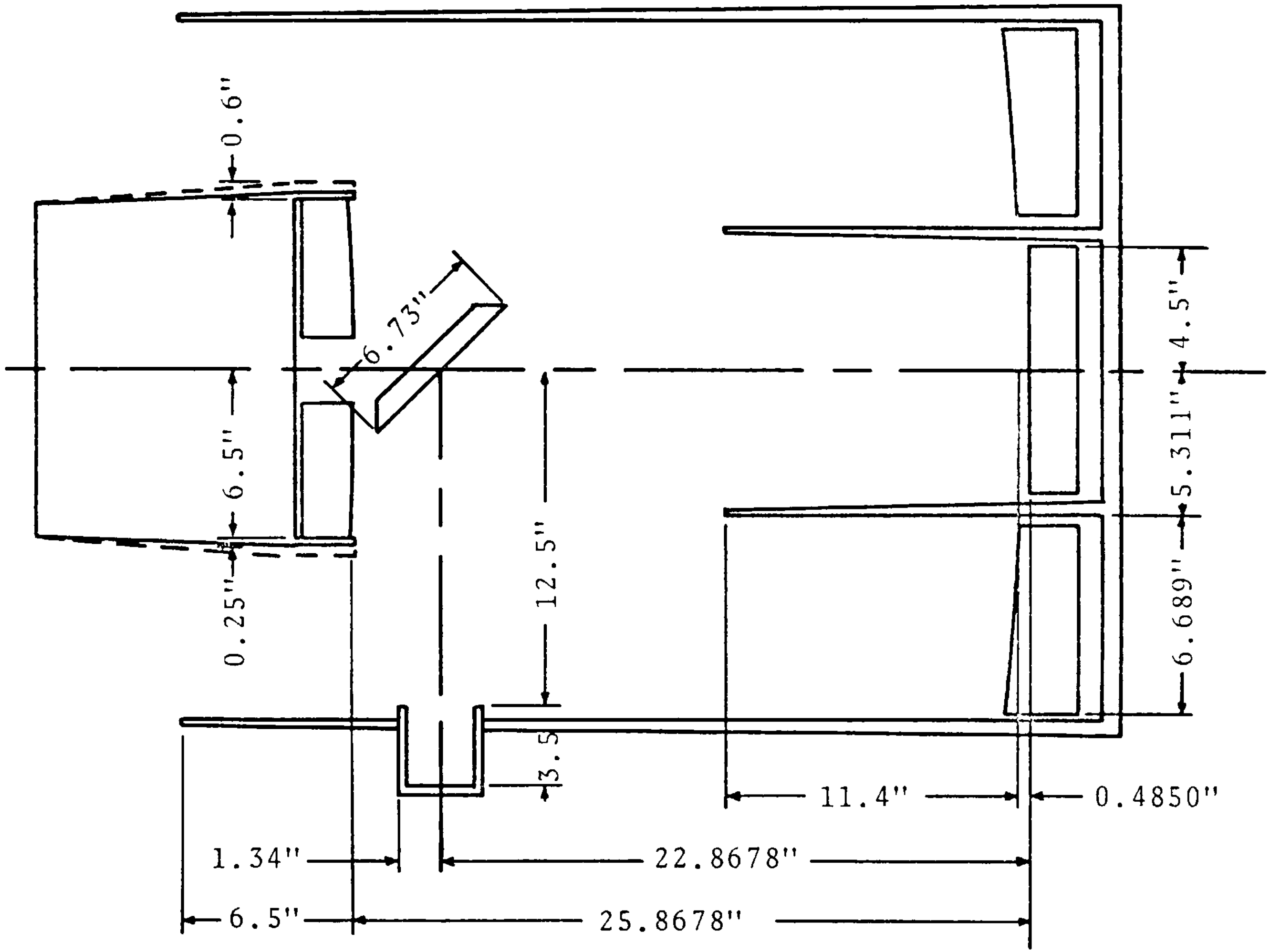

Fig. 12. Scale Drawing of Final System

CHAPTER 6

MANUFACTURING ERRORS AND THEIR EVALUATION

Unavoidable errors which occur during fabrication will cause a degradation in the performance of the final system. An observable effect of this degradation on the image of a point source is a spreading out of the light beyond the predicted distribution for the ideal design. In addition, the spreading may be unsymmetric and will vary over the image plane. This results in a blurring in the fine detail of the image of an object.

Types of Errors

The image degradation is caused by several kinds of fabrication errors. Among these are tilt and displacement of a surface. A tilt is a slight rotation of the surface about both the x and y axes of a coordinate system located at the point where the surface intercepts the optic axis. A displacement is a slight displacement in the x,y plane of the vertex of the surface from the origin of the coordinate system. Errors can also occur in the spacing, curvature, and aspheric correction of a surface. These consist of slight deviations from the design values. Another source of error is localized, random changes in curvature over a surface. These can occur during the polishing and figuring stages of manufacture and are the result of localized action by the polishing tool. Since localized polishing is commonly used to generate aspherics, this type of error may be significant in systems with highly aspheric surfaces. These errors are all small, but they do degrade the performance of the system.

Requirements of a System Performance Criterion

Before considering the effects of errors, we must first decide on a method of evaluating the system. Now, there are several criterion in use today which describe the performance of optical systems. Some of these are spot diagrams, RMS spot size, and optical transfer functions (OTF). The first two listed are purely geometrical calculations which do not consider the effects of diffraction. For high performance designs, it is quite possible to have the spot size smaller than the airy disc. This implies that the image of a point source is smaller than that predicted by diffraction theory. In particular, the design selected for this study has a spot size about one tenth that of the airy disc. Figure 13 shows the on axis spot diagram for the final design. Comparison with Figure 7 shows that diffraction has the major effect on the point image. For this reason, diffraction effects must be considered.

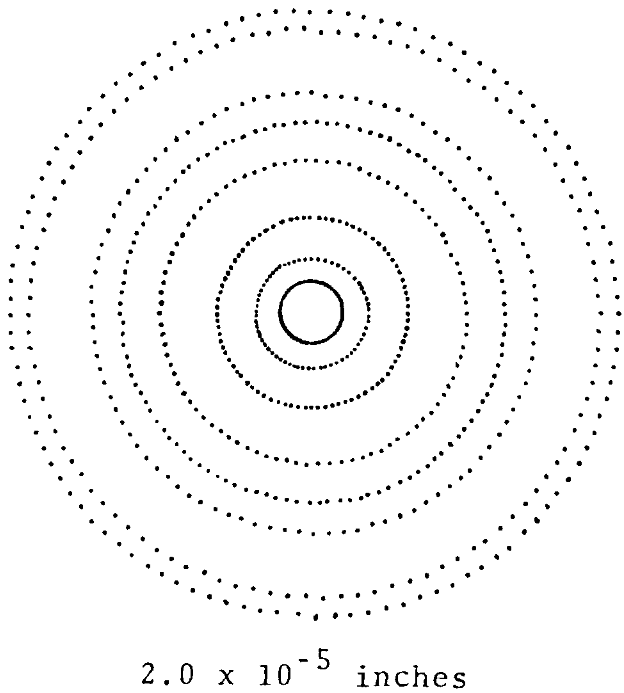

Fig. 13. On Axis Spot Diagram for Final Design

The diameter of the spot diagram is about one-tenth that of the core of the point spread function (Fig. 7).

The optical transfer function can be computed either on a geometric or a diffraction basis. Basically, the OTF describes the ability of a system to image objects with sinusoidal intensity distributions. If we assume an object consisting of alternating light and dark bands with a sinusoidal brightness distribution, then we can describe the distribution by

$$G(\chi) = b_0 + b_1 \cos 2\pi \upsilon \chi . \tag{6.1}$$

Where b_0 is a DC brightness level, b_1 is the amplitude of the brightness change, and υ is the spatial frequency of the brightness variation. It is measured in cycles per unit length. The maximum brightness is $b_0 + b_1$, and the minimum is $b_0 - b_1$. Now, modulation, M, is defined as

$$M = \frac{b_{max} - b_{min}}{b_{max} + b_{min}} . \tag{6.2}$$

From this, the modulation of the object, M_o, is

$$M_o = \frac{b_1}{b_0} . \tag{6.3}$$

Since each point in the object is imaged as a finite sized spot, the modulation of the image, M_i, will be decreased. The ratio of the modulation in the image to that in the object as a function of the spatial frequency is termed the

Modulation Transfer Function (MTF) and is denoted by $\tau(\upsilon)$.

$$\tau(\upsilon) = \frac{M_i}{M_o} \tag{6.4}$$

In the case that the point spread function is asymmetric, the sinusoidal image will be displaced an amount Δ from its geometrically determined position. We can express this displacement as a phase shift, $\phi(\upsilon)$, in the sinusoid.

$$\phi(\upsilon) = 2\pi\upsilon\Delta(\upsilon) \tag{6.5}$$

The optical transfer function describes both the modulation and phase shift of the imagery of sinusoidal objects as a function of spatial frequency.

Transfer functions are becoming increasingly popular in the evaluation of complete photographic systems. One reason for this is that two or more transfer functions may be easily cascaded. For example, we can multiply the camera MTF by the MTF of a film to get the resultant MTF of the combination. Another reason is that they provide an objective measurement of the imagery produced by the system (Shannon 1965). These functions can completely describe the image produced if they are known in several azimuths at several field positions and several focal planes. Figure 14 is a plot of the MTF for two aberration free systems (Smith 1966). One has no central obscuration and the other has an obscuration ratio of 0.5. We see that the

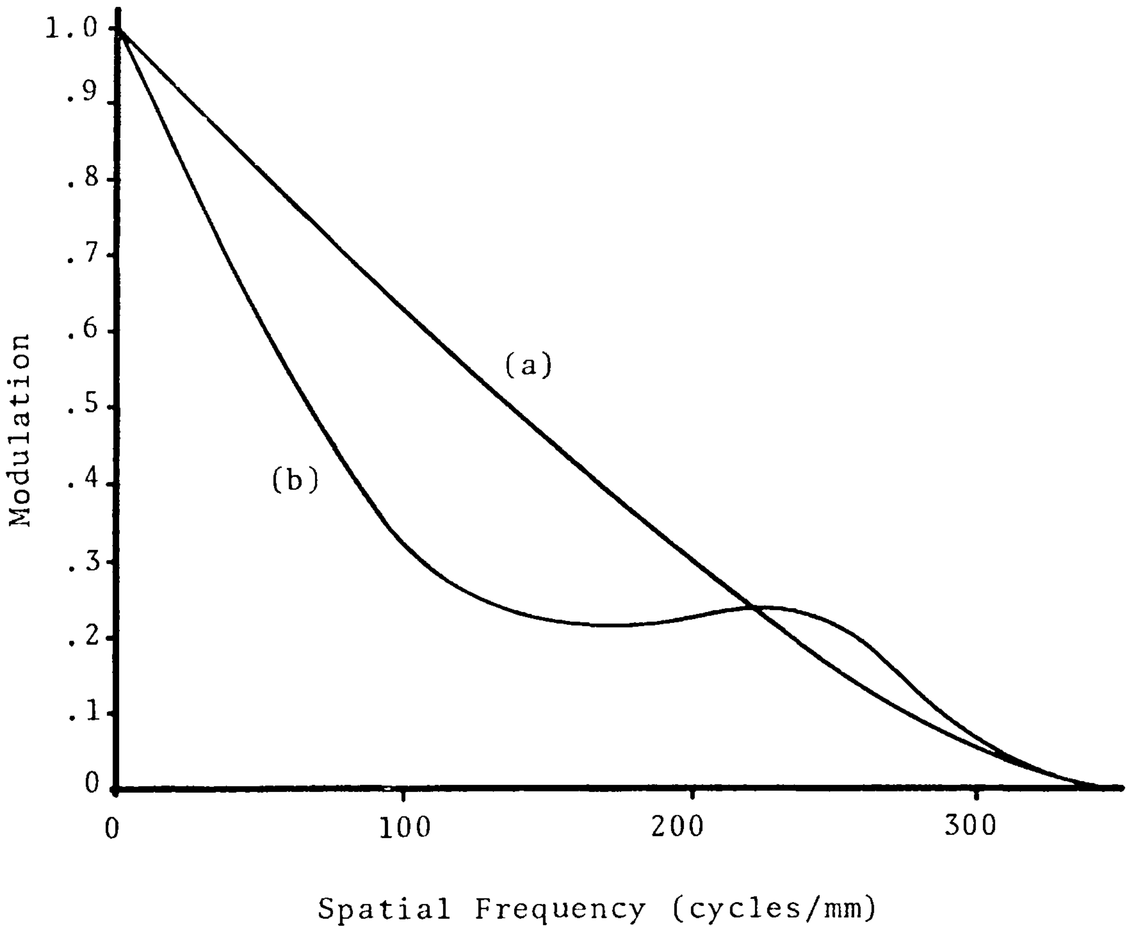

Fig. 14. Effect of Obscuration Ratio on MTF
For curve a, ρ=0.0, and for b, ρ=0.5.

addition of a central obscuration causes the modulation in the lower and midfrequencies to be reduced. However, the modulation in the higher frequencies is slightly increased. The reduced modulation is further evidence of the need for a low obscuration ratio.

Methods of Error Evaluation

Once we have selected a performance criteria, we would then like to know what would be the effect of manufacturing errors on that criteria. We can be sure the image will be degraded, but by what factor is an obvious question to ask. Furthermore, this knowledge should allow us to assign a confidence factor to the system. That is, we would like to know what percentage of fabricated systems will perform at a specified level or higher. Ideally, this would be predicted from a knowledge of the design and the probability distribution of errors which an optician will make. The probability distribution is a plot of the probability of making an error of a given magnitude versus the magnitude. Suppose our performance test is RMS spot size, and we know that the distribution of tilts and decenters is given by two functions $g(\theta)$ and $h(x,y)$ with limits θ_1, θ_2, x_1, y_1, x_2 and y_2. Then, through appropriate mathematical manipulations of $g(\theta)$ and $h(x,y)$ with the ray tracing equations we would get a distribution function, H, for the RMS spot size. Generally, the shape and limits of H would be functions of the shapes and limits of $g(\theta)$ and $h(x,y)$. We may suppose that larger limits on the error distribution functions would result in a greater spread and lower levels in the performance distribution of the system. This type of approach would give the distribution of performance levels of many fabricated systems.

Another approach to the problem of manufacturing errors can be used. This consists of deliberately changing the design values of the ideal design by a slight amount and then calculating the resultant performance of the altered design. By determining the performance of many altered designs with random errors in them, we can then approximate the probability distribution of the performance criterion.

The choice of the random errors must be done with care. Let us assume that we are going to evaluate a hundred altered designs and that all errors are present at each surface. Now, each kind of error, such as tilt, will have a probability distribution g_t, with specified limits. The subscript "t" designates tilt. We can form a list of one hundred numbers with the same distribution and limits as g_t. From that list, we pick a number at random and assign it to the tilt error on the ideal design. We continue doing this for the remaining designs, being careful not to repeat a number, until they all have assigned errors. The result is one hundred altered designs with the same distribution of tilt errors at the first surface as might be expected of one hundred manufactured systems. Repeating the above procedure for all types of errors at each surface, results in a hundred mathematical models of the kinds of fabricated systems which we can expect to encounter in practice. We can then plot the probability distribution of their performance levels.

Clearly, the procedure outlined in the preceding paragraph would be time-consuming and expensive. The selection of lists of numbers with the proper distributions would be a formidable task in itself. Furthermore, this approach yields only an approximation to the probability distribution of performance levels.

Because of the disadvantages of the second approach, the first one which was outlined is preferred. Unfortunately, such a technique has not been worked out in detail. For this reason and the disadvantages of the second approach, a modified form of the second approach was used for this report. In this approach, the emphasis is changed from finding a distribution of performance numbers to establishing the maximum tolerable errors we can allow and still expect reasonable performance.

The basic strategy is to establish several groups of maximum allowable errors and then evaluate the performance of a few altered designs within each group. A group of maximum allowable errors consists of a collection of numbers which are the limits of the error distribution function for each type of error. A single group therefore, consists of ten numbers which are the upper and a lower limits for each of the five types of errors. Different groups simply have different values for the limits. Five altered systems are evaluated using errors chosen randomly from a group. The evaluations then give an indication of how much degradation to expect when a system is constructed with tolerances established by the corresponding group.

Selection of Errors

The basis for establishing the limits within a group was simply experience. The group with the largest range was based on easily obtained, reasonable tolerances. For spacing and centering of the surfaces, this is $\pm$ 0.001 inch. Limits on tilts were established by relating it to a spacing measurement. A measure of the tilt is the axial distance, Δ, that the rim of a surface is displaced from the plane which was established by the rim when the surface was centered on the optic axis and normal to it. The tilt angle, θ, is then

$$\theta = {}^{2\Delta}/_{D} ,$$

where D is the diameter of the surface. In this way, we can relate the maximum tilt to the maximum spacing and centering errors. A reasonable maximum curvature error was obtained by consulting with the optical shop. For the primary and secondary, an error of $\pm$ 0.25 inch in the radius of curvature was considered attainable. The maximum error for the long radius of the tertiary was set at $\pm$ 50.0 inches. The limits for changes in aspheric coefficients were based on the amount of change needed in the fourth order aspheric coefficient to alter the sag of the surface a given amount at its rim. The amount of sag change for the most liberal case was one fifth wavelength.

Three different error groups were established for the report. They were labeled A, B and C respectively. The limits for A were the most liberal. The limits for B and C respectively were one half and one fifth those of group A. An exception is that the curvature and aspheric error limits for C were unchanged from B. Table II is a list of the limits for each surface in each error group.

Besides limits, the shape of the error distribution functions must also be determined. Due to a lack of any experimentally derived curves and to be pessimistic, an equal probability for any size error, between the limits, was assumed. That is, the probability distribution for errors is a "box-car" function.

TABLE II

Range of Limits for Error Groups

Error Group A

Error		Primary	Secondary	Tertiary
Spacing (inches)		±0.001	±0.001	—
Decenter, x-direction (inches)		±0.001	±0.001	—
Decenter, y-direction (inches)		±0.001	±0.001	—
Tilt about x-axis (10^{-4} radians)		±0.800	±1.550	±2.220
Tilt about y-axis (10^{-4} radians)		±0.800	±1.550	±2.220
Radius of curvature (inches)		±0.250	±0.250	±50.0
Aspheric term	AD	$\pm 0.0020 \times 10^{-07}$	$\pm 0.0026 \times 10^{-06}$	$\pm 0.0028 \times 10^{-06}$
	AE	$\pm 0.0010 \times 10^{-11}$	$\pm 0.0012 \times 10^{-09}$	$\pm 0.0090 \times 10^{-10}$
	AF	$\pm 0.0010 \times 10^{-14}$	$\pm 0.0022 \times 10^{-12}$	$\pm 0.0045 \times 10^{-11}$
	AG	$\pm 0.0060 \times 10^{-17}$	$\pm 0.0042 \times 10^{-14}$	$\pm 0.0017 \times 10^{-12}$

TABLE II (Continued)

Error Group B

Error		Primary	Secondary	Tertiary
Spacing (inches)		±0.0005	±0.0005	—
Decenter, x-direction (inches)		±0.0005	±0.0005	—
Decenter, y-direction (inches)		±0.0005	±0.0005	—
Tilt about x-axis (10^{-4} radians)		±0.40	±0.78	±1.11
Tilt about y-axis (10^{-4} radians)		±0.40	±0.78	±1.11
Radius of curvature (inches)		±0.125	±0.125	±12.500
Aspheric term	AD	$\pm0.0010\times10^{-07}$	$\pm0.0013\times10^{-06}$	$\pm0.0028\times10^{-06}$
	AE	$\pm0.0005\times10^{-11}$	$\pm0.0006\times10^{-09}$	$\pm0.0090\times10^{-10}$
	AF	$\pm0.0005\times10^{-14}$	$\pm0.0011\times10^{-12}$	$\pm0.0045\times10^{-11}$
	AG	$\pm0.0030\times10^{-17}$	$\pm0.0021\times10^{-14}$	$\pm0.0017\times10^{-12}$

TABLE II (Continued)

Error Group C

Type of Error		Primary	Secondary	Tertiary
Spacing (inches)		±0.0002	±0.0002	—
Decenter, x-direction (inches)		±0.0002	±0.0002	—
Decenter, y-direction (inches)		±0.0002	±0.0002	—
Tilt about x-axis (10^{-4} radians)		±0.16	±0.31	±0.44
Tilt about y-axis (10^{-4} radians)		±0.16	±0.31	±0.44
Radius of curvature (inches)		±0.125	±0.125	±12.500
Aspheric term	AD	$\pm 0.0010 \times 10^{-07}$	$\pm 0.0013 \times 10^{-06}$	$\pm 0.0028 \times 10^{-06}$
	AE	$\pm 0.0005 \times 10^{-11}$	$\pm 0.0006 \times 10^{-09}$	$\pm 0.0090 \times 10^{-10}$
	AF	$\pm 0.0005 \times 10^{-14}$	$\pm 0.0011 \times 10^{-12}$	$\pm 0.0045 \times 10^{-11}$
	AG	$\pm 0.0030 \times 10^{-17}$	$\pm 0.0021 \times 10^{-14}$	$\pm 0.0017 \times 10^{-12}$

Five ideal designs were assigned to each error group. For each type of error at each surface, five numbers were chosen at random. The maximum size of each number was established by the error group limits in Table II. To insure that the five numbers for each error did fit a box-car function, two tests were made. One test required their sum to be nearly zero, and the other required the average value of their absolute magnitudes to be about half the magnitude of the limit. Each number was then assigned to the corresponding error in each of the five ideal designs. This resulted in fifteen altered designs with all types of errors at each surface. Table III lists the actual errors used in each of the systems in the three error groups. Table IV describes the effects of the errors on the wavefront. The numbers given are the optical path differences between the vertex and rim of a surface which is caused by the corresponding errors in Table III.

Computation of the OTF

The actual determination of the OTF for a system with errors in it is difficult. The basic computational techniques of H.H. Hopkins and J.L. Rayces were used for this thesis. They were incorporated into a computer program called Program for the Analysis of General Optical Systems (PAGOS). The program was written by Mr. S.H. Brewer and Mr. B.J. Gold, for the Aerospace Corporation.

TABLE III

Errors Used in Tests

Group A

System#	Δr_1 (in)	Δr_2 (in)	Δr_3 (in)	Δd_{12} (10^{-3} in)	Δd_{23} (10^{-3} in)
1	+0.160208	+0.188418	-24.67162	-0.7671	-0.3076
2	+0.231373	-0.039015	-38.00951	+0.2103	+0.7286
3	-0.127574	-0.234656	+50.73571	+0.7334	-0.9777
4	+0.093495	+0.128617	+15.04309	-0.6766	+0.1769
5	+0.055905	-0.039992	- 7.73932	+0.3227	+0.3835

System#	ΔAD_1	ΔAD_2	ΔAD_3
1	-0.0018354×10^{-7}	$+0.0014998\times10^{-6}$	$+0.0014558\times10^{-6}$
2	$+0.0009788\times10^{-7}$	-0.0021643×10^{-6}	$+0.0012440\times10^{-6}$
3	-0.0008075×10^{-7}	$+0.0012224\times10^{-6}$	-0.0010640×10^{-6}
4	$+0.0015227\times10^{-7}$	-0.0010257×10^{-6}	$+0.0027311\times10^{-6}$
5	$+0.0001551\times10^{-7}$	$+0.0004743\times10^{-6}$	-0.0025085×10^{-6}

TABLE III (Continued)

Errors Used in Tests

Group A

System#	$DLTX_1$ (10^{-4} in)	$DLTY_1$ (10^{-4} in)	$DLTX_2$ (10^{-4} in)	$DLTY_2$ (10^{-4} in)	$DLTX_3$ (10^{-4} in)	$DLTY_3$ (10^{-4} in)
1	+2.1795	+8.2964	-9.2215	-3.4714	8.0217	-4.5432
2	+7.3956	-2.5915	+5.9611	+5.1518	+4.2739	-2.0132
3	-4.1421	-6.8719	-4.6446	-6.9237	-7.3414	+6.0907
4	-7.5017	-3.8389	+1.0124	-2.3428	-2.3940	+5.5881
5	+3.7811	+3.4041	+4.8874	+7.1986	-3.5249	-5.5884

System#	$THTX_1$ (10^{-4} rad)	$THTY_1$ (10^{-4} rad)	$THTX_2$ (10^{-4} rad)	$THTY_2$ (10^{-4} rad)	$THTX_3$ (10^{-4} rad)	$THTY_3$ (10^{-4} rad)
1	-0.2467	+0.6051	-1.4491	-0.5197	+2.1560	-0.5320
2	+0.6627	-0.3674	+0.6224	-0.0481	-0.1324	+1.3040
3	-0.7793	-0.5896	-0.2998	-0.6606	+0.9073	+1.0458
4	+0.1816	+0.3780	+0.2415	-0.5554	-1.4342	-1.9937
5	+0.2255	-0.1117	-0.2464	+1.8651	-1.1301	+0.6893

TABLE III (Continued)

Errors Used in Tests

Group B

System#	Δr_1 (in)	Δr_2 (in)	Δr_3 (in)	Δd_{12} (10^{-3} in)	Δd_{23} (10^{-3} in)
1	-0.063305	+0.022946	+15.18192	+0.1835	+0.1565
2	+0.033608	+0.075763	+ 6.63048	+0.4734	-0.2887
3	+0.102177	-0.043098	-22.46318	-0.3394	+0.4542
4	-0.085534	+0.058871	-19.48829	-0.2368	-0.2841
5	-0.022953	-0.114955	+ 1.18866	-0.0902	-0.1569

System#	ΔAD_1	ΔAD_2	ΔAD_3
1	$+0.0008037\times10^{-7}$	$+0.0012133\times10^{-6}$	-0.0007896×10^{-6}
2	-0.0005433×10^{-7}	-0.0007617×10^{-6}	$+0.0021491\times10^{-6}$
3	$+0.0003440\times10^{-7}$	-0.0009443×10^{-6}	$+0.0009595\times10^{-6}$
4	-0.0006634×10^{-7}	-0.0010601×10^{-6}	$+0.0007250\times10^{-6}$
5	$+0.0001632\times10^{-7}$	$+0.0003561\times10^{-6}$	-0.0013917×10^{-6}

TABLE III (Continued)

Errors Used in Tests

Group B

System#	$DLTX_1$ (10^{-4} in)	$DLTY_1$ (10^{-4} in)	$DLTX_2$ (10^{-4} in)	$DLTY_2$ (10^{-4} in)	$DLTX_3$ (10^{-4} in)	$DLTY_3$ (10^{-4} in)
1	-1.7608	+4.3422	+2.4464	-1.6021	-3.6549	+4.9952
2	-3.9404	+1.3244	-4.2638	-4.4488	+4.1434	+1.7011
3	+2.4922	-0.3924	-0.6124	+0.5909	+1.7553	-3.8988
4	+4.3223	-2.4661	-1.2413	+4.3311	-1.7333	-0.1304
5	-1.0168	-2.4961	+3.9044	+1.5485	-1.3212	-1.6601

System#	$THTX_1$ (10^{-4} rad)	$THTY_1$ (10^{-4} rad)	$THTX_2$ (10^{-4} rad)	$THTY_2$ (10^{-4} rad)	$THTX_3$ (10^{-4} rad)	$THTY_3$ (10^{-4} rad)
1	+0.1042	+0.3909	-0.2282	+0.5251	+0.7349	-0.1055
2	+0.3884	+0.0562	-0.2331	-0.2511	-1.0083	+0.1551
3	-0.3947	-0.2918	+0.3359	-0.3016	+0.3270	+0.6969
4	+0.0244	-0.2433	-0.4929	+0.5536	-0.4648	-0.7608
5	-0.1191	+0.0322	+0.7184	-0.5063	+0.2822	+1.0112

TABLE III (Continued)

Errors Used in Tests

Group C

System#	Δr_1 (in)	Δr_2 (in)	Δr_3 (in)	Δd_{12} (10^{-3} in)	Δd_{23} (10^{-3} in)
1	-0.019408	-0.031568	+8.013498	+0.1030	-0.1319
2	+0.022517	+0.026142	+4.822328	+0.1526	+0.1008
3	-0.006796	-0.020792	-4.332402	-0.0105	+0.0735
4	-0.031016	-0.015443	-6.49224	-0.0582	-0.1359
5	+0.036804	+0.035884	-2.312542	-0.1724	+0.1136

System#	ΔAD_1	ΔAD_2	ΔAD_3
1	$+0.0008037\text{x}10^{-7}$	$+0.0012133\text{x}10^{-6}$	$-0.0007896\text{x}10^{-6}$
2	$-0.0005433\text{x}10^{-7}$	$-0.0006617\text{x}10^{-6}$	$+0.0021491\text{x}10^{-6}$
3	$+0.0003440\text{x}10^{-7}$	$-0.0009443\text{x}10^{-6}$	$+0.0009595\text{x}10^{-6}$
4	$-0.0006634\text{x}10^{-7}$	$-0.0010601\text{x}10^{-6}$	$+0.0007250\text{x}10^{-6}$
5	$+0.0001632\text{x}10^{-7}$	$+0.0003561\text{x}10^{-6}$	$-0.0013917\text{x}10^{-6}$

TABLE III (Continued)

Errors Used in Tests

Group C

System#	$DLTX_1$ (10^{-4} in)	$DLTY_1$ (10^{-4} in)	$DLTX_2$ (10^{-4} in)	$DLTY_2$ (10^{-4} in)	$DLTX_3$ (10^{-4} in)	$DLTY_3$ (10^{-4} in)
1	-0.5761	+1.4835	-0.0092	+1.4487	-0.7376	-0.0813
2	-0.4296	-1.5455	-1.2523	+1.3764	-1.0909	+1.1528
3	-1.1313	+0.2781	-1.0558	-0.0697	-0.5624	-0.6969
4	-1.0575	-0.6941	-0.8839	-0.5682	+1.1090	+1.5264
5	+1.8262	+1.1528	+1.7745	-1.6742	+1.7900	-1.5481

System#	$THTX_1$ (10^{-4} rad)	$THTY_1$ (10^{-4} rad)	$THTX_2$ (10^{-4} rad)	$THTY_2$ (10^{-4} rad)	$THTX_3$ (10^{-4} rad)	$THTY_3$ (10^{-4} rad)
1	+0.0782	-0.1249	+0.2702	+0.2288	-0.3941	+0.2751
2	+0.1428	+0.0139	+0.0929	+0.0218	+0.0202	-0.1434
3	-0.0816	+0.1379	-0.1535	-0.2739	-0.2156	-0.2311
4	-0.1119	+0.0014	-0.2118	-0.0259	+0.1132	+0.2645
5	-0.0077	-0.1285	+0.0756	+0.1702	+0.3249	-0.1212

TABLE IV

Effect of Errors on Wavefront

Error Group A

System#	$\frac{\Delta r_1}{\lambda}$	$\frac{\Delta r_2}{\lambda}$	$\frac{\Delta r_3}{\lambda}$	$\frac{\Delta d_{12}}{\lambda}$	$\frac{\Delta d_{23}}{\lambda}$
1	+41.332	+13.755	-0.162	-0.818	-0.083
2	-59.693	- 2.848	-0.250	+0.224	+0.197
3	-32.913	-17.130	+0.333	+0.782	-0.264
4	+24.122	+ 9.389	+0.100	-0.721	+0.048
5	+14.423	- 2.919	-0.050	+0.344	+0.104

System#	$\frac{\Delta AD_1}{\lambda}$	$\frac{\Delta AD_2}{\lambda}$	$\frac{\Delta AD_3}{\lambda}$
1	-0.1671	+0.1177	+0.0266
2	+0.0893	-0.1693	+0.0223
3	-0.0735	+0.0964	-0.0197
4	+0.1381	-0.0802	+0.0508
5	+0.1412	+0.0371	-0.0451

TABLE IV (Continued)

Effect of Errors on Wavefront

Error Group A

System#	DLTX$_1$ λ	DLTY$_1$ λ	DLTX$_2$ λ	DLTY$_2$ λ	DLTX$_3$ λ	DLTY$_3$ λ
1	+1.020	+3.884	-2.321	-0.874	+0.054	-0.031
2	+3.463	-1.213	+1.500	+1.297	+0.029	-0.014
3	-1.939	-3.217	-1.169	-1.743	-0.049	+0.041
4	-3.512	-1.797	+0.255	-0.590	-0.016	+0.038
5	±1.770	+1.594	+1.230	+1.812	-0.024	-0.038

System#	THTX$_1$ λ	THTY$_1$ λ	THTX$_2$ λ	THTY$_2$ λ	THTX$_3$ λ	THTY$_3$ λ
1	-12.965	+31.799	-41.249	-14.793	+40.600	-10.018
2	+34.826	-19.307	+17.717	- 1.369	- 2.493	+24.555
3	-40.954	-30.984	+36.999	-18.804	+17.085	+19.693
4	+ 9.543	+19.865	- 6.874	-15.810	-27.007	-37.543
5	+11.850	- 5.870	- 7.014	+53.090	-21.281	+12.980

TABLE IV (Continued)

Effect of Errors on Wavefront

Error Group B

System#	Δr_1 λ	Δr_2 λ	Δr_3 λ	Δd_{12} λ	Δd_{23} λ
1	-16.333	+1.675	+0.100	+0.199	+0.042
2	+ 8.671	+5.531	+0.043	+0.505	-0.078
3	+26.336	-3.146	-0.148	-0.362	+0.123
4	-22.068	+4.298	-0.128	-0.252	-0.077
5	- 5.922	-3.392	+0.008	-0.096	-0.042

System#	ΔAD_1 λ	ΔAD_2 λ	ΔAD_3 λ
1	+0.073	+0.095	-0.014
2	-0.049	-0.060	+0.039
3	+0.031	-0.074	+0.017
4	-0.060	-0.083	+0.013
5	+0.015	+0.028	-0.025

TABLE IV (<u>Continued</u>)

Effect of Errors on Wavefront

Error Group B

System#	$DLTX_1$ λ	$DLTY_1$ λ	$DLTX_2$ λ	$DLTY_2$ λ	$DLTX_3$ λ	$DLTY_3$ λ
1	-0.824	+2.033	+0.616	-0.403	-0.025	+0.034
2	-1.845	+0.620	-1.073	-1.120	+0.028	+0.011
3	+1.167	-0.184	-0.154	+0.149	+0.012	-0.026
4	+2.024	-1.155	-0.312	+1.090	-0.012	-0.001
5	-0.476	-1.169	+0.983	+0.390	-0.009	-0.011

System#	$THTX_1$ λ	$THTY_1$ λ	$THTX_2$ λ	$THTY_2$ λ	$THTX_3$ λ	$THTY_3$ λ
1	+ 5.476	+20.542	- 6.496	+14.947	+13.839	- 1.987
2	+20.411	+ 2.953	- 6.635	- 7.148	-18.987	+ 2.921
3	-20.742	-15.335	+ 9.561	- 8.585	+ 6.158	+13.123
4	+ 1.282	-12.786	-14.030	+15.758	- 8.753	-14.326
5	- 6.259	+ 1.692	+ 5.078	-14.412	+ 5.314	+19.042

TABLE IV (Continued)

Effect of Errors on Wavefront

Error Group C

System#	Δr_1 λ	Δr_2 λ	Δr_3 λ	Δd_{12} λ	Δd_{23} λ
1	-5.007	-2.304	+0.053	+0.110	-0.036
2	+5.809	+1.952	+0.032	+0.163	+0.027
3	-1.753	-1.518	-0.028	-0.011	+0.020
4	-8.002	-1.127	-0.043	-0.062	-0.037
5	+9.495	+2.620	-0.015	-0.184	+0.031

System#	ΔAD_1 λ	ΔAD_2 λ	ΔAD_3 λ
1	+0.073	+0.095	-0.014
2	-0.049	-0.052	+0.039
3	+0.031	-0.074	+0.017
4	-0.060	-0.083	+0.013
5	+0.015	+0.028	-0.025

TABLE IV (Continued)

Effect of Errors on Wavefront

Error Group C

System#	$DLTX_1$ λ	$DLTY_1$ λ	$DLTX_2$ λ	$DLTY_2$ λ	$DLTX_3$ λ	$DLTY_3$ λ
1	-0.270	+0.695	-0.002	+0.365	-0.005	-0.001
2	-0.201	-0.724	-0.315	+0.346	-0.007	+0.008
3	-0.053	+0.130	-0.266	-0.018	-0.004	-0.005
4	-0.495	-0.325	-0.222	-0.143	+0.007	+0.010
5	+0.855	+0.540	+0.045	-0.042	+0.012	-0.010

System#	$THTX_1$ λ	$THTY_1$ λ	$THTX_2$ λ	$THTY_2$ λ	$THTX_3$ λ	$THTY_3$ λ
1	+4.109	-6.564	+7.691	+6.513	-7.421	+5.180
2	+7.504	+0.730	+2.644	+0.621	+0.380	-2.700
3	-4.288	+7.247	-4.369	-7.797	-4.060	-4.352
4	-5.881	+0.074	-6.029	-0.737	+2.132	+4.981
5	-0.405	-6.753	+2.152	+4.845	+6.118	-2.282

PAGOS has the ability to compute, on a diffraction basis, the optical transfer function for a wide variety of systems. It is fairly suitable for the evaluation of manufacturing errors because it has the capacity to include tilts and displacements of any surface. Spacing, curvature, and aspheric coefficient errors may be introduced by altering the design values. However, no provision is made to include random, localized surface errors. Figure 15 is a plot of the on-axis MTF for the final system as computed by PAGOS. Included, for comparison, is the MTF for an aberration free system with the same obscuration ratio as the final system.

Prediction of Resolving Power of a Fabricated System

A method has been described by G.C. Brock to predict the resolving power of a camera when used with a film (Brock 1965). This method uses curves which describe the emulsion resolving power as a function of target modulation. The curves are obtained by imaging standard U.S. Air Force three-bar targets of various modulations on the emulsion. A plot of the modulation necessary to achieve a resolvable image versus the inverse of the bar spacing (cycles/mm) is then constructed. This is called the aerial film modulation threshold. The aerial film modulation thresholds for three different emulsions are plotted in Figure 16. The plots were published by the Eastman Kodak Company. To

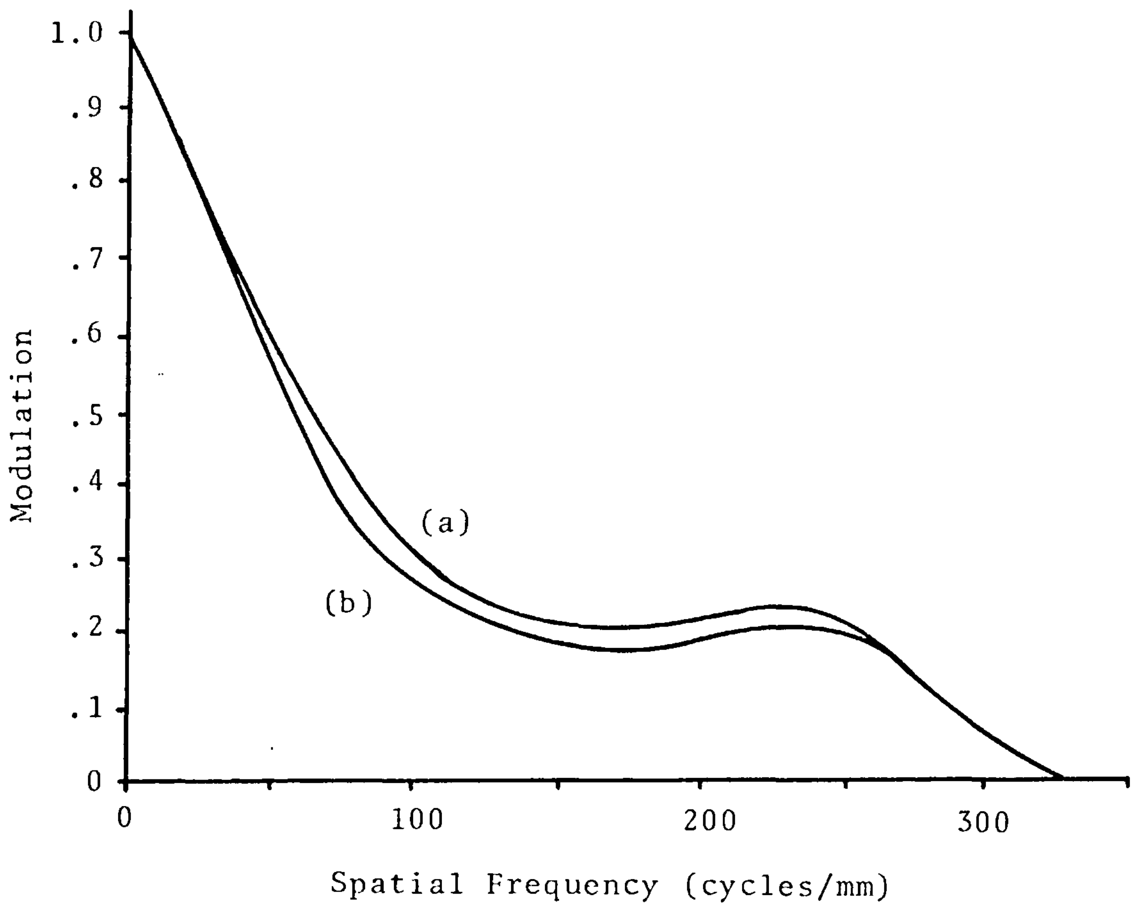

Fig. 15. Comparison of MTF for (a) Aberration Free System with That of Ideal Design (b)

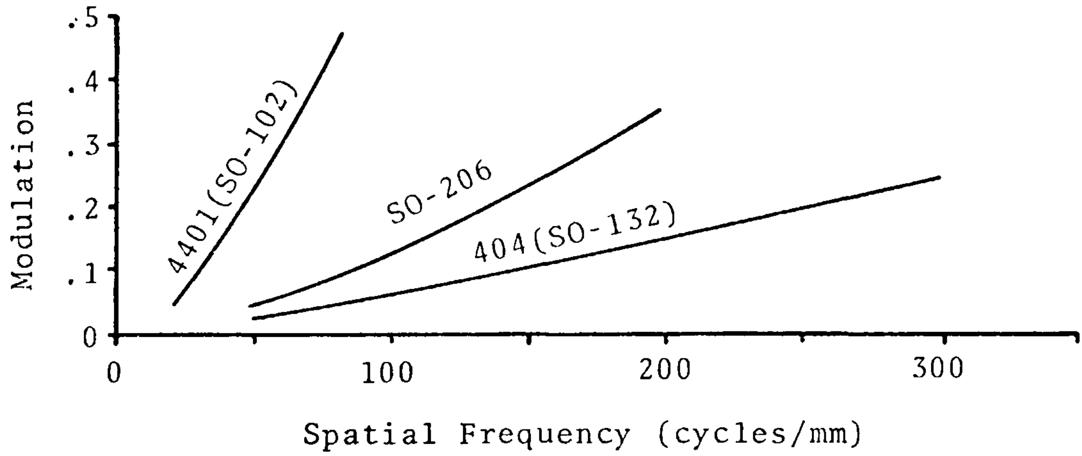

Fig. 16. Aerial Film Modulation Thresholds

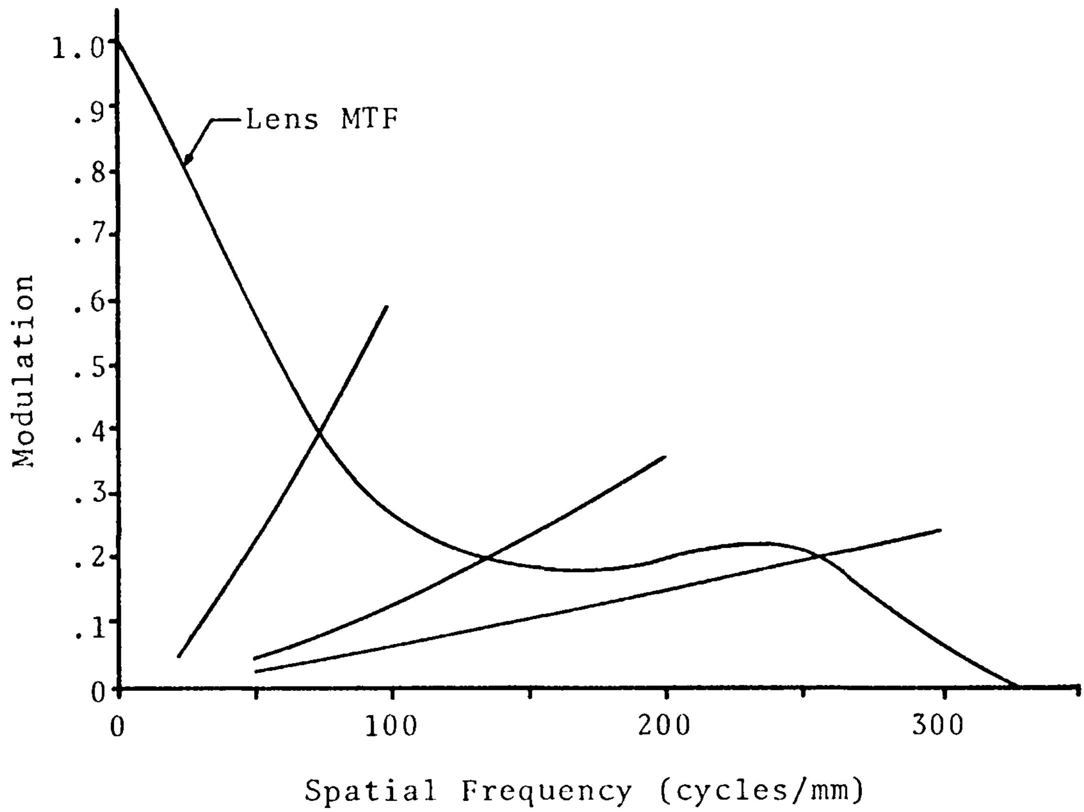

Fig. 17. Prediction of Resolving Power

obtain the resolving power, draw the camera MTF on the plots in Figure 16. At the point where the camera MTF crosses each threshold curve, the aerial image contrast equals the contrast required by the emulsion. This point establishes the resolving power of the camera-film combination. An example of this is shown in Figure 17.

The value for the resolving power obtained in this manner should be used only with caution. The threshold curves of Figure 16 were produced under a special set of circumstances. The curves apply to development in D-19 at an exposure level that gives maximum resolving power. Equivalent results under other circumstances should not be expected.

CHAPTER 7

RESULTS

This chapter consists of plots of the Modulation Transfer Functions for the designs described in chapters 4, 5 and 6. These designs include the theoretical ideal designs and those with various manufacturing errors. The modulation for each plot is normalized to one. The abcissa of all the plots is labeled spatial frequency. The scale for the abcissa can be determined from the cut off frequency of the system. The spatial frequency where the modulation drops to zero is called the cut off frequency, μ_{co}, and it is given by the formula,

$$\mu_{co} = \frac{1}{\lambda \text{ f-number}} . \qquad (7.1)$$

In the calculation of the MTF, the value of the wavelength which was used was

$$\lambda = 0.58 \ \mu m .$$

For an f-number of five, the cut off frequency becomes

$$\mu_{co} = 340 \text{ lines/mm} .$$

The plots in the following figures indicate a lower cut off frequency than 340 lines/mm. This was caused by an unknown factor in the computer program. The cut off frequency as given by the computer, μ'_{co}, can be approximated by,

$$\mu'_{co} = \frac{23}{24}\,\mu_{co}\ . \qquad (7.2)$$

This equation may be used to scale the abcissa so that the MTF at any wavelength may be determined from the following plots.

MTFs for the Ideal Design

Figures 18 through 22 compare the MTFs for designs C and D. The plots are given in the sagittal and tangential directions, for three field points. The figures show that design C has a higher MTF than D for spatial frequencies below 250 cycles/mm.

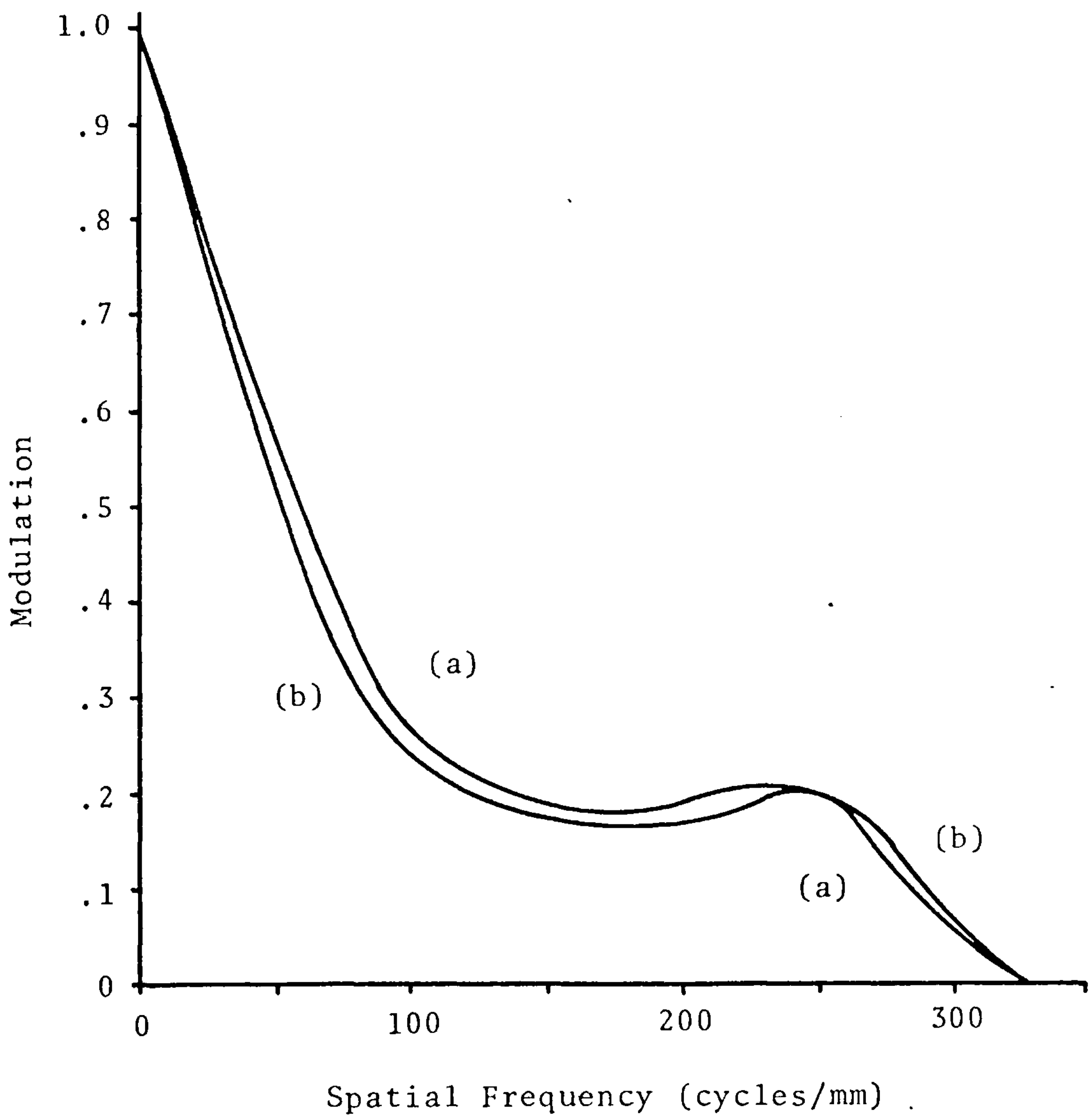

Fig. 18. Comparison of On-Axis MTF for (a) Design C and (b) Design D

Both plots are for the ideal theoretical designs.

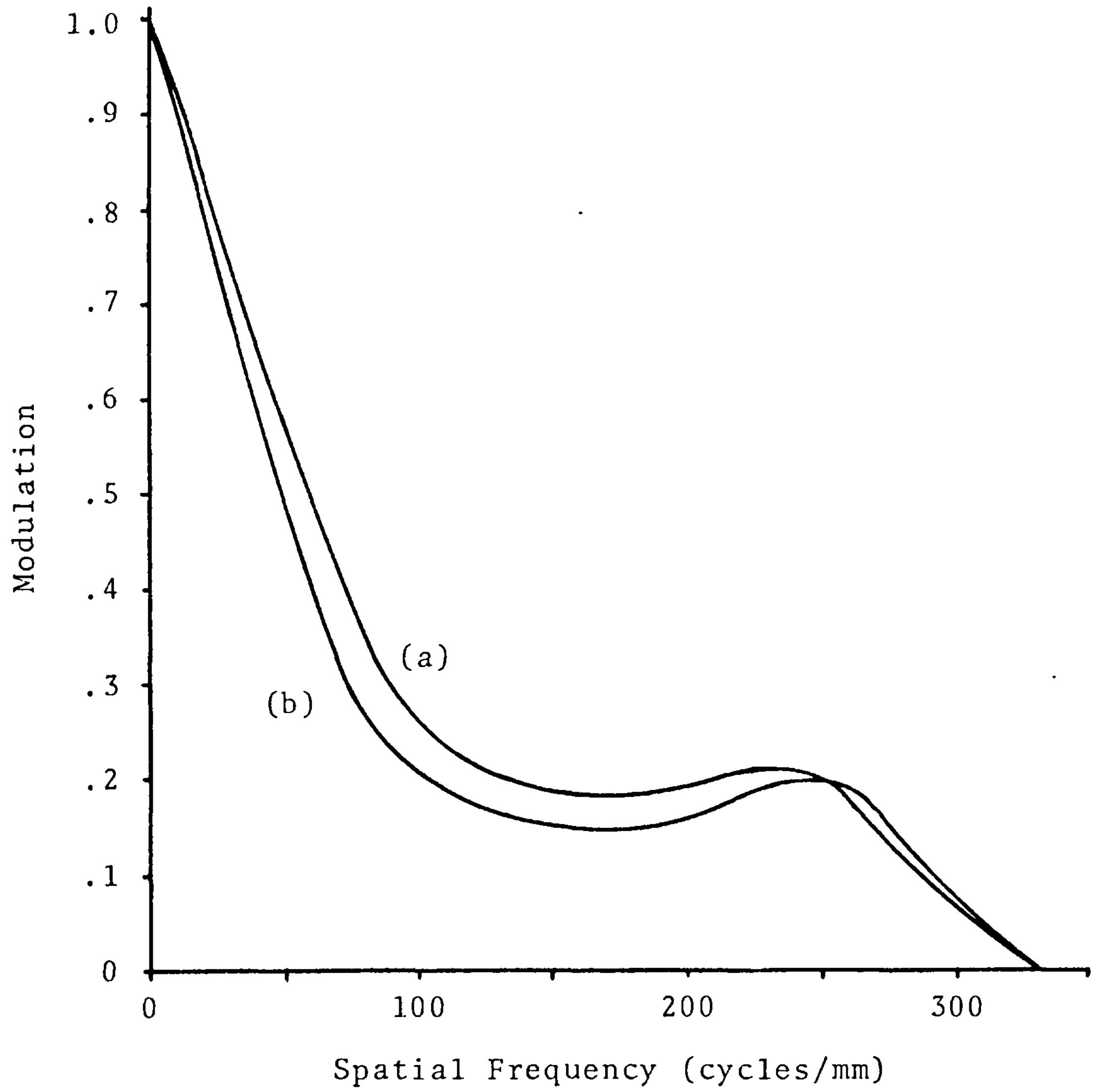

Fig. 19. Sagittal MTF at Half-Field for (a) Design C and (b) Design D

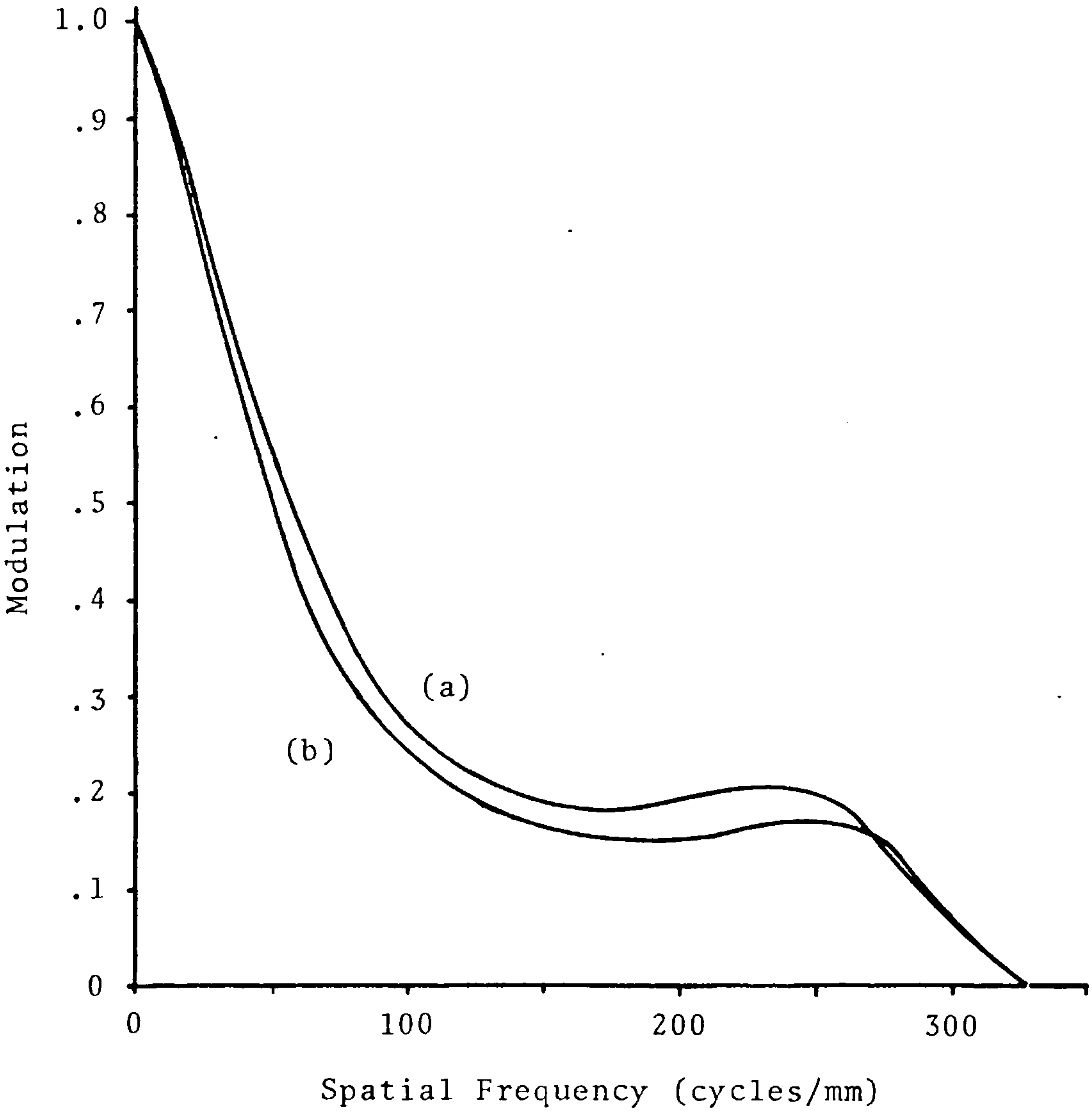

Fig. 20. Tangential MTF at Half-Field for (a) Design C and (b) Design D

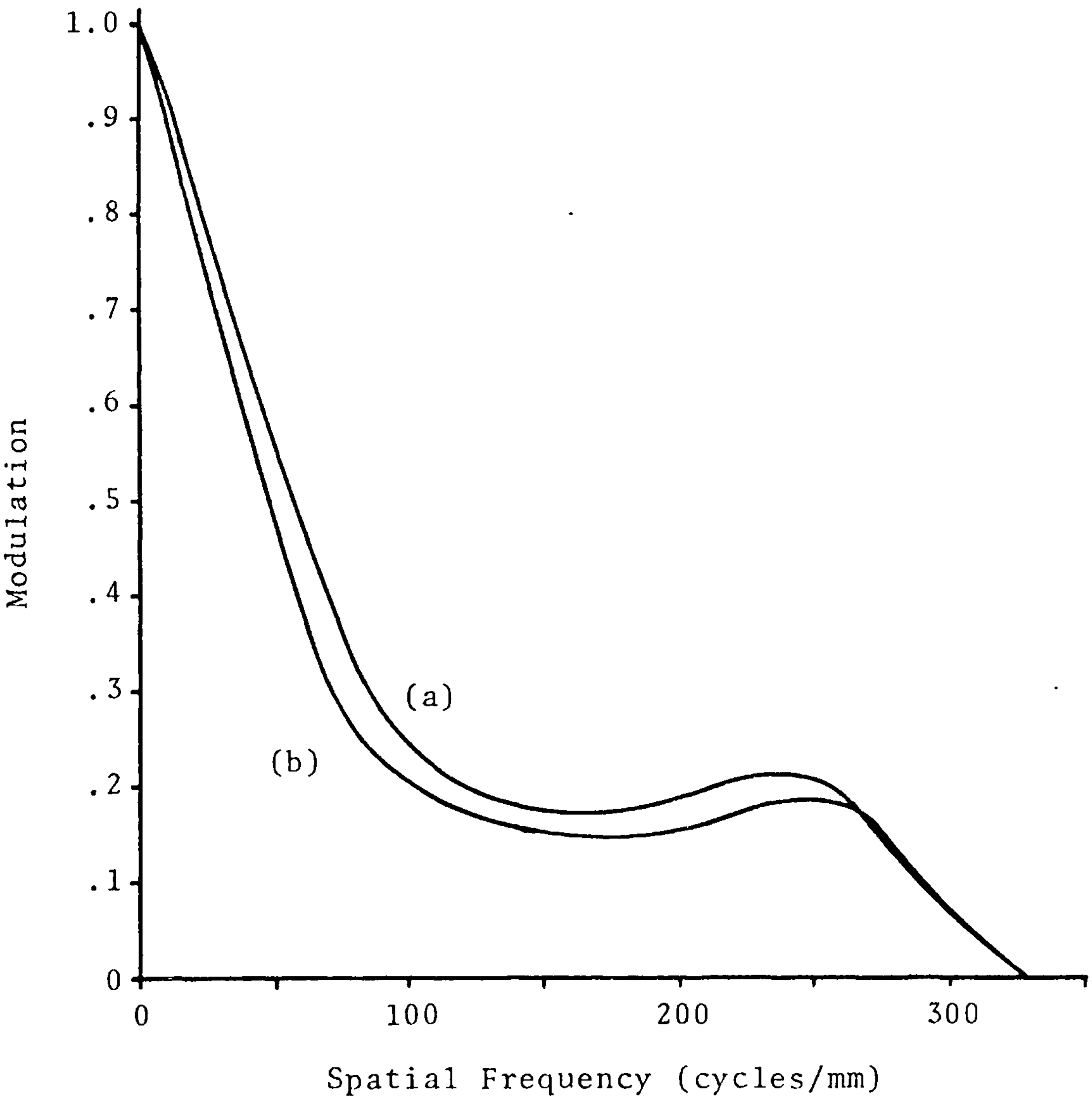

Fig. 21. Sagittal MTF at Full-Field for (a) Design C and (b) Design D

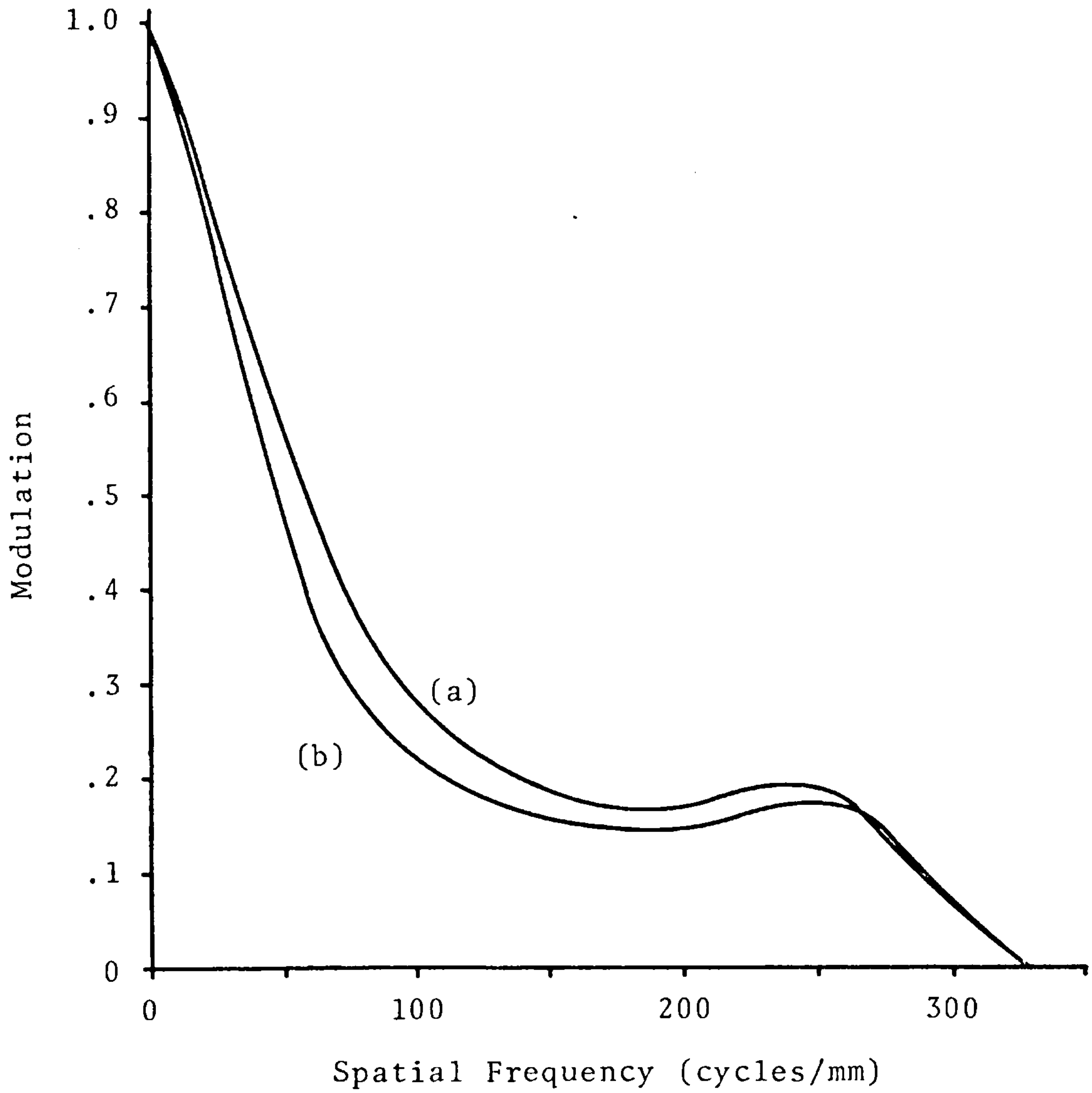

Fig. 22. Tangential MTF at Full-Field for (a) Design C and (b) Design D

MTFs for Error Groups A, B and C

Figures 23 through 26 describe the MTF of design C with manufacturing errors from group A in it. The first figure shows the tangential MTFs for each of the five aberrated systems considered. Both the modulus and phase are plotted. The phase shifts were plotted in radians. The second figure shows the sagittal MTFs for the five systems. The average values of the five tangential and sagittal MTFs are shown in figures 25 and 26. Also, the transfer factors of the average MTFs are plotted in these figures as functions of spatial frequency. These transfer factors are the ratio of the average MTF to the ideal MTF as a function of spatial frequency. The short vertical lines indicate the average difference between the individual MTFs and the average MTF. In the same manner, figures 27 through 30 and 31 through 34 describe the effects of error groups B and C respectively on the performance of design C.

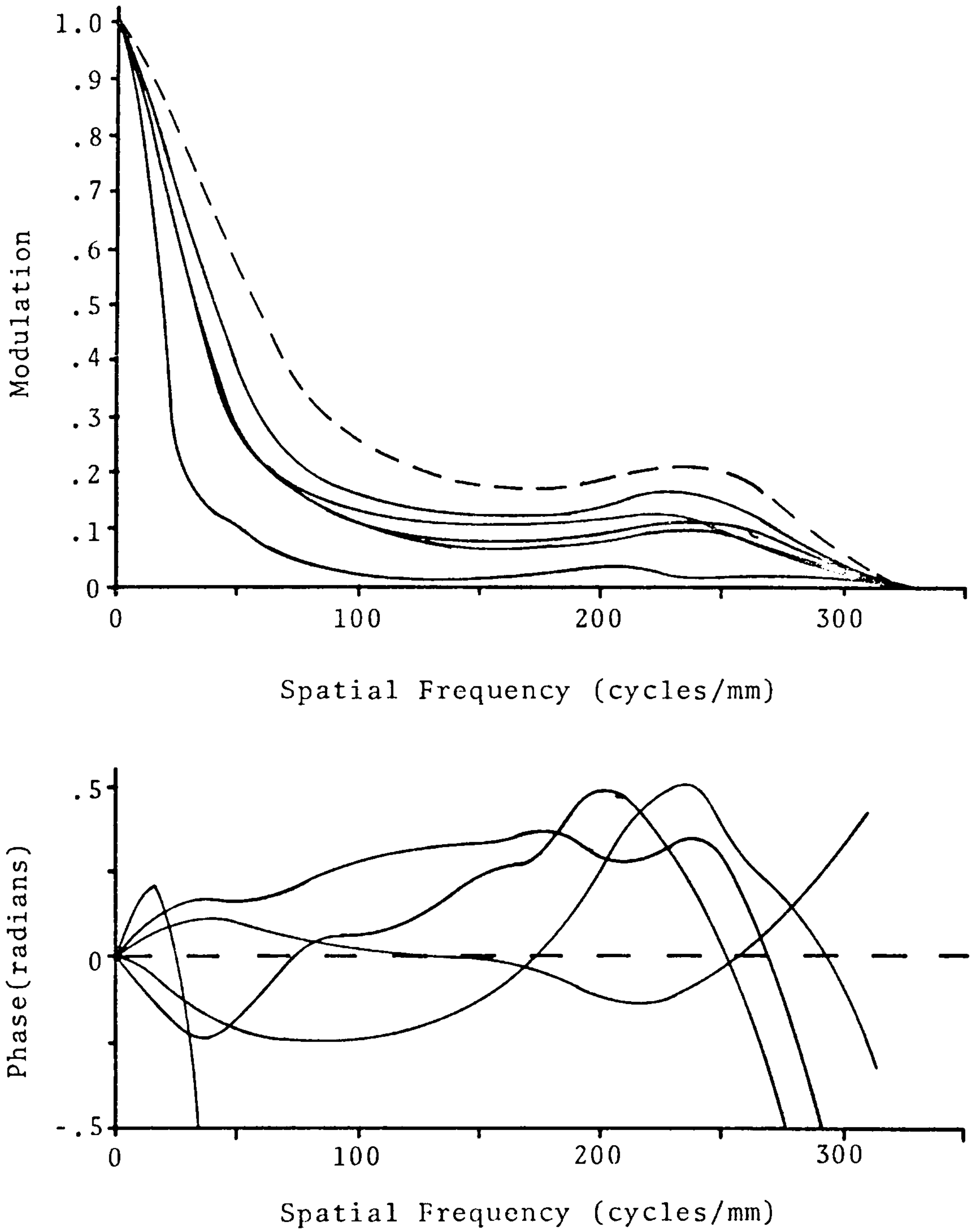

Fig. 23. Sagittal MTFs at Full-Field for Error Group A.

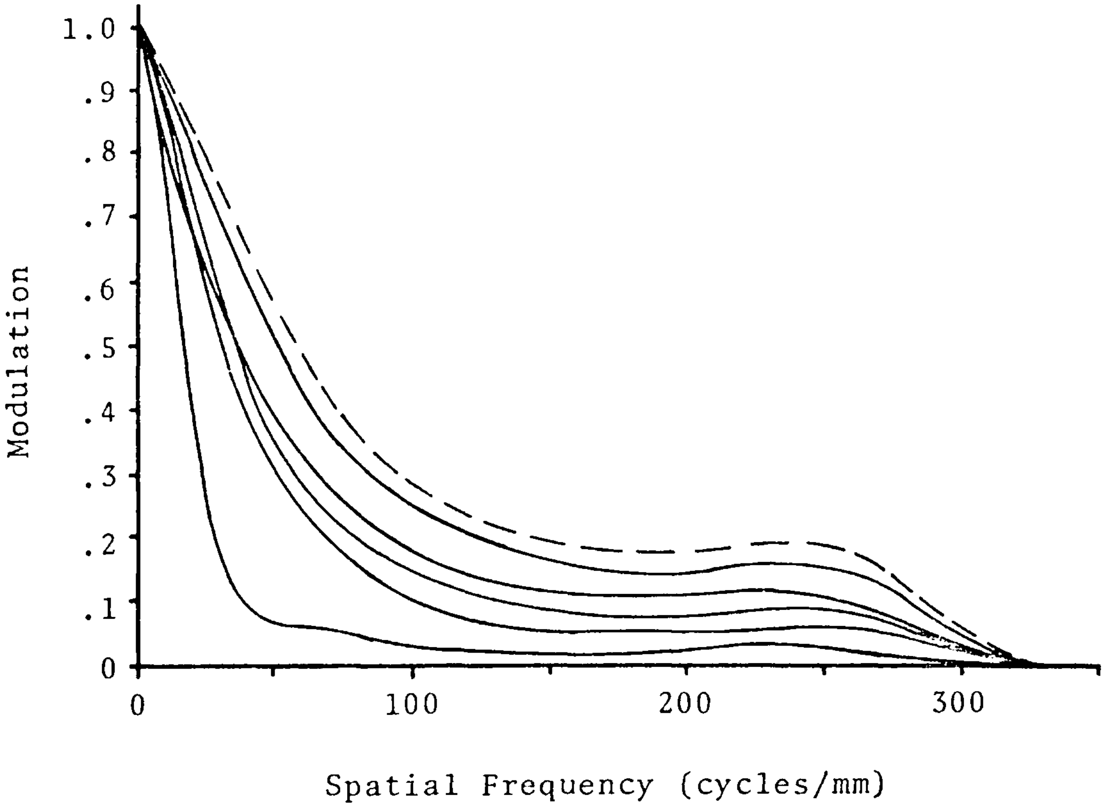

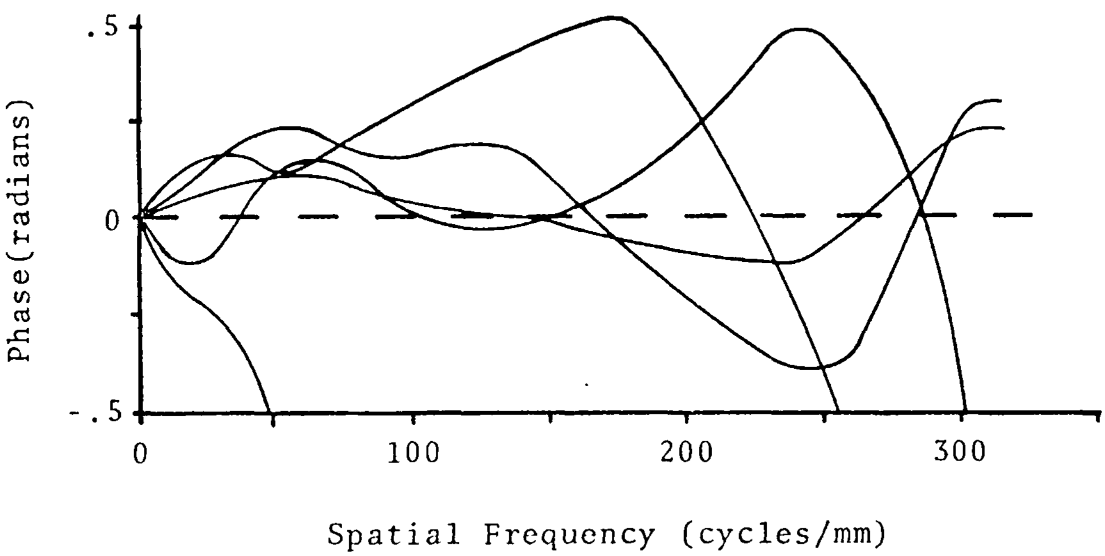

Fig. 24. Tangential MTFs at Full-Field for Error Group A.

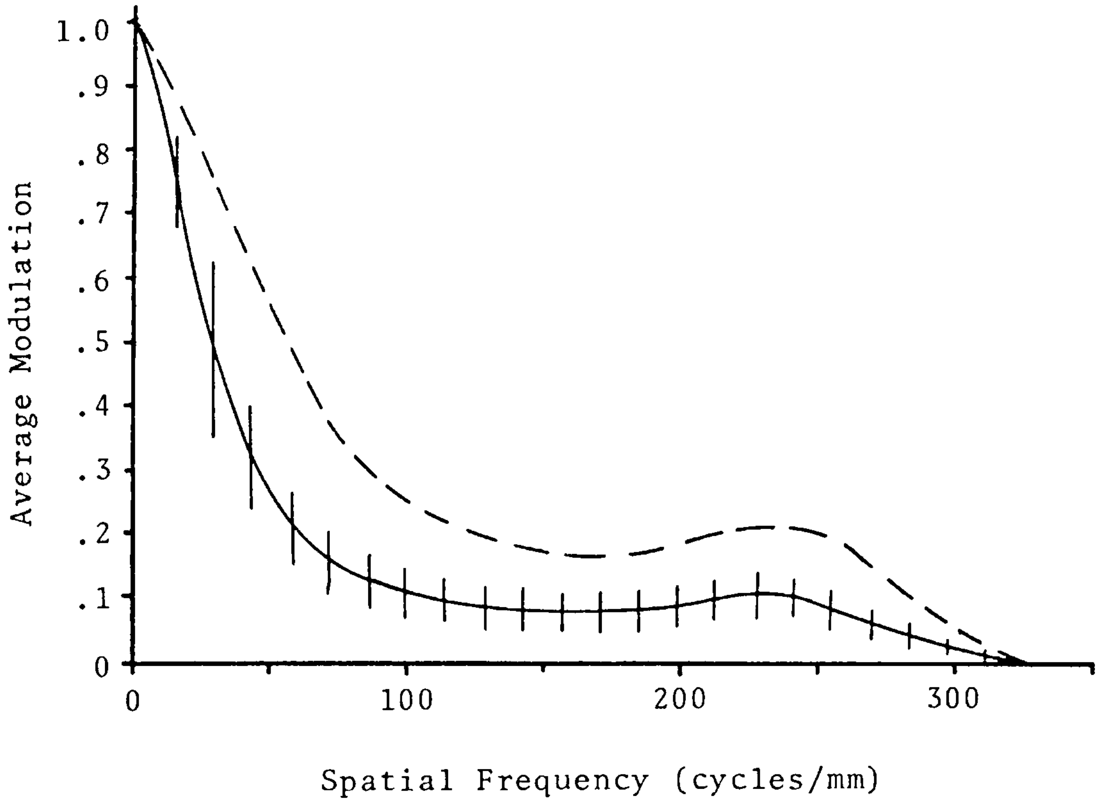

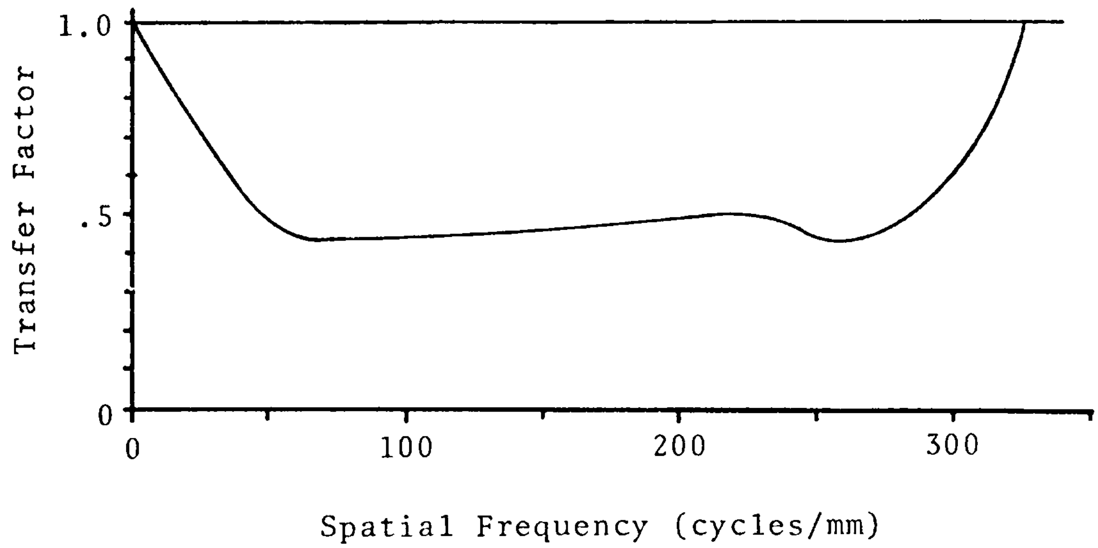

Fig. 25. Average Sagittal MTF at Full-Field for Error Group A.

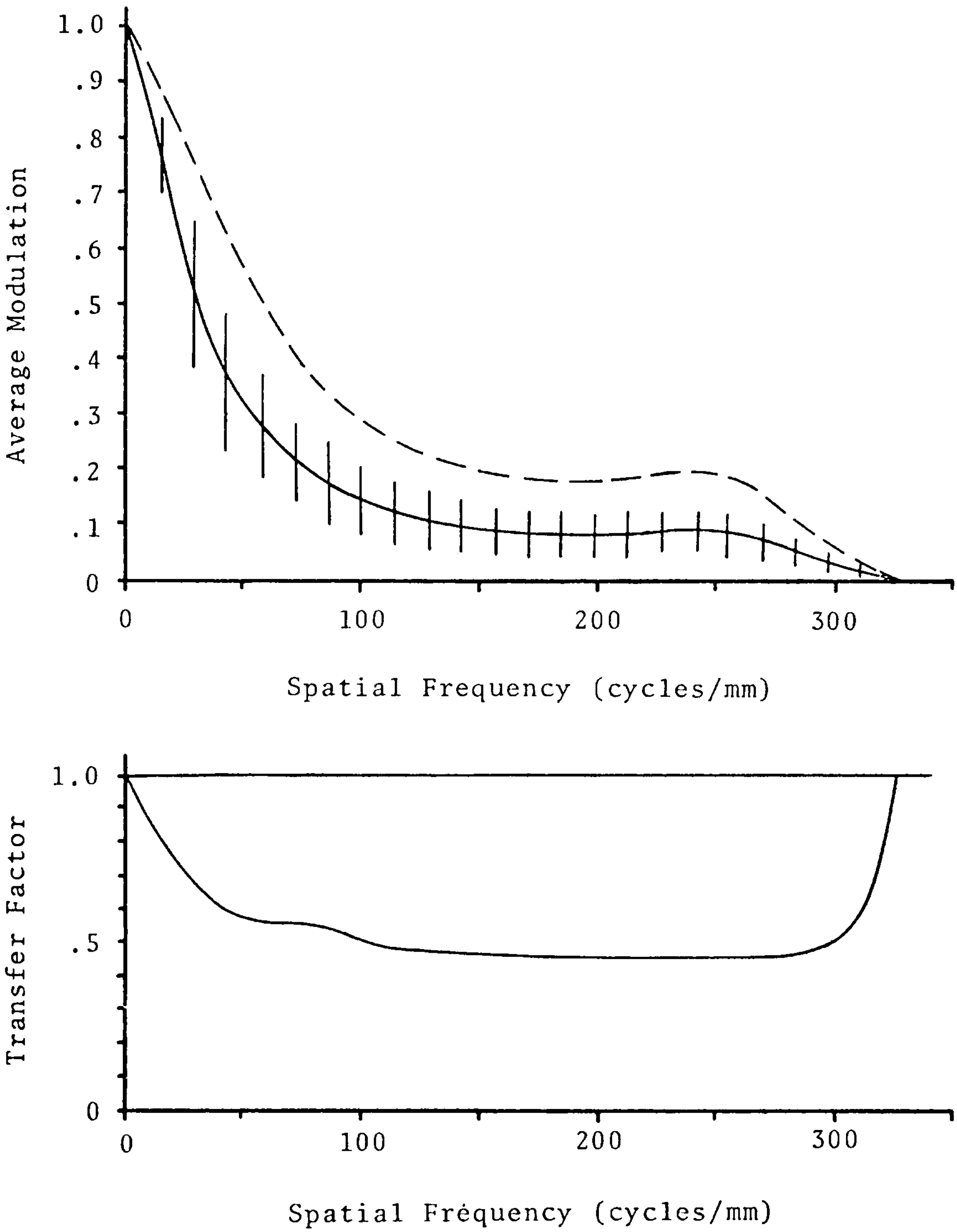

Fig. 26. Average Tangential MTF at Full-Field for Error Group A.

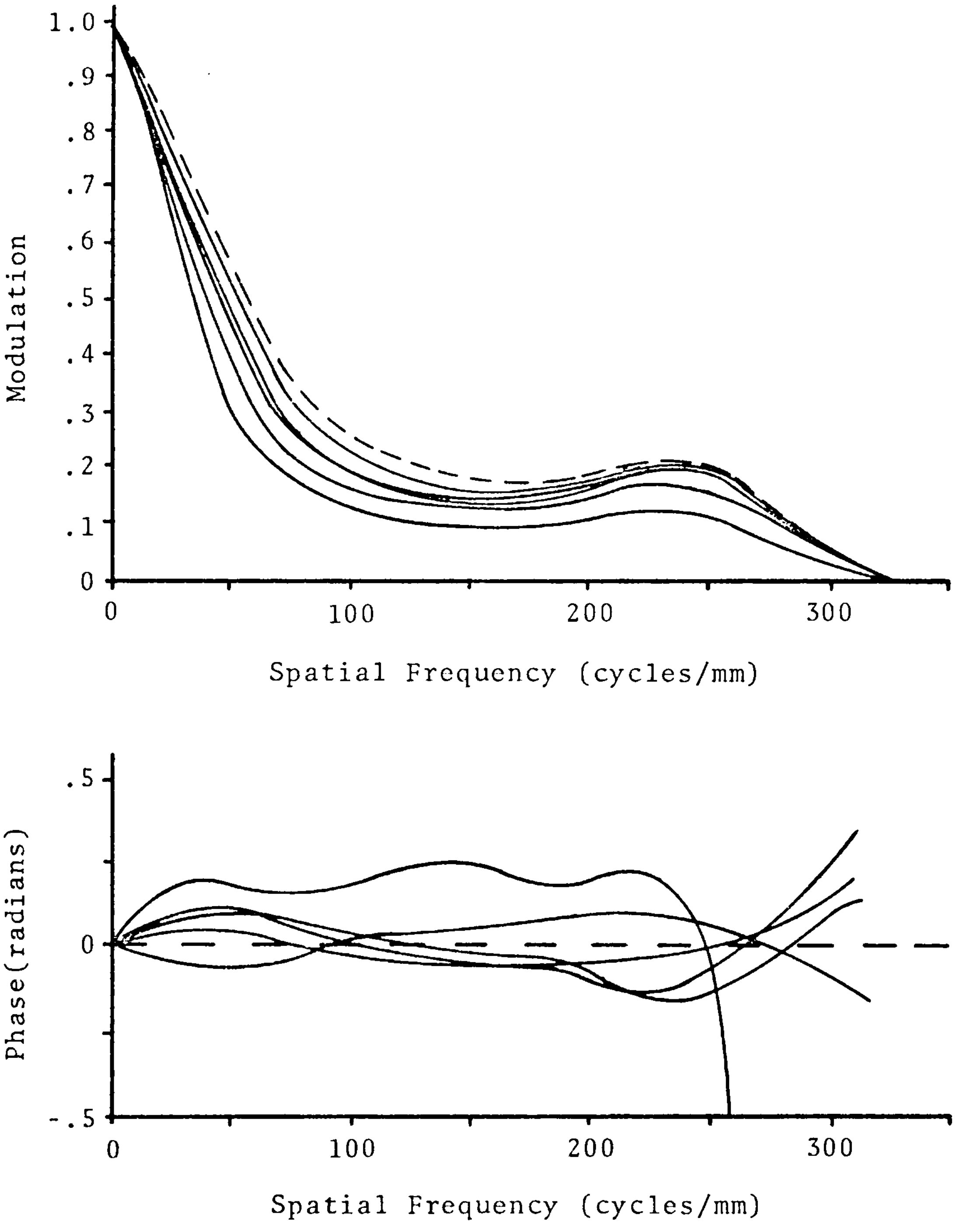

Fig. 27. Sagittal MTFs at Full-Field for Error Group B.

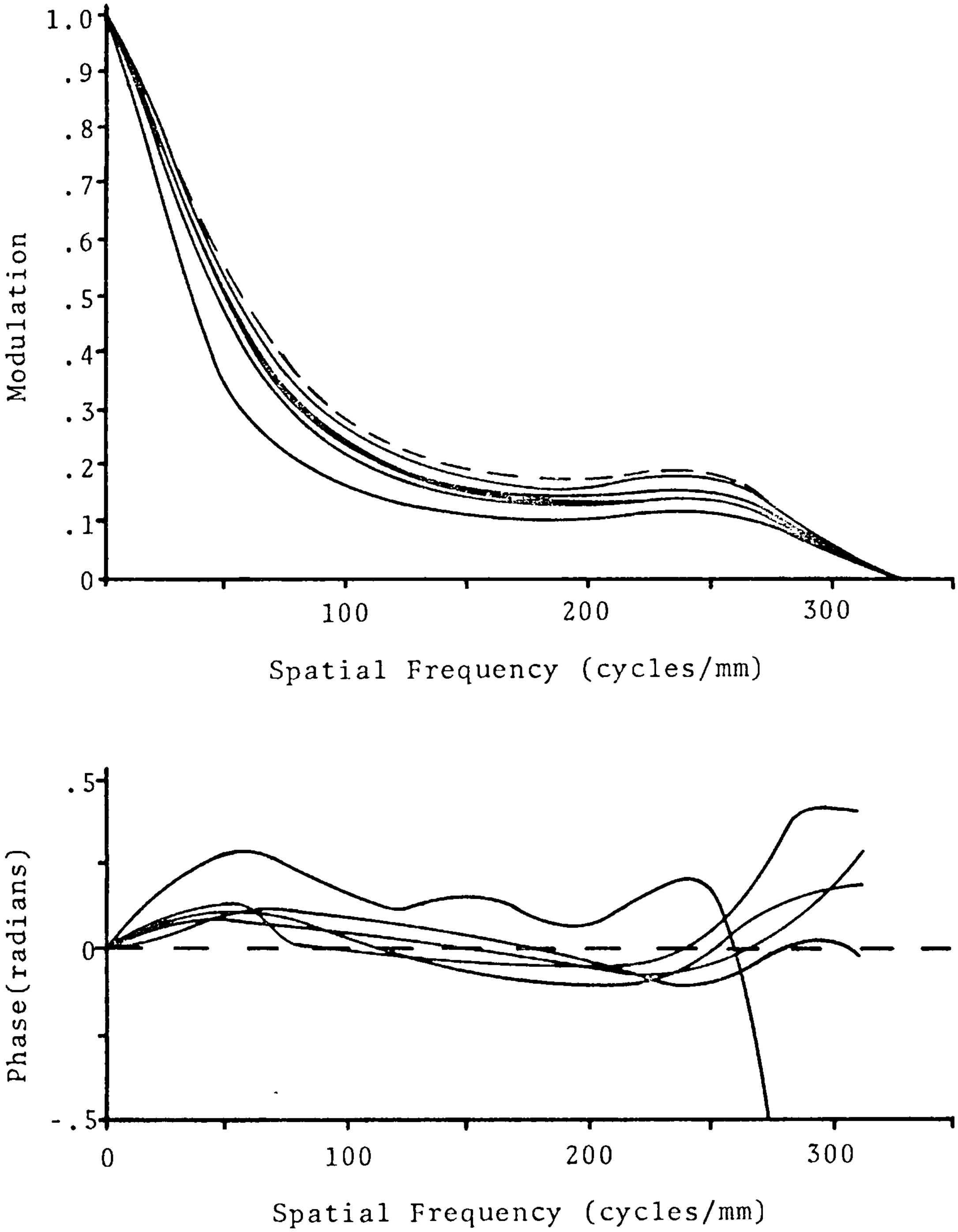

Fig. 28. Tangential MTF at Full-Field for Error Group B.

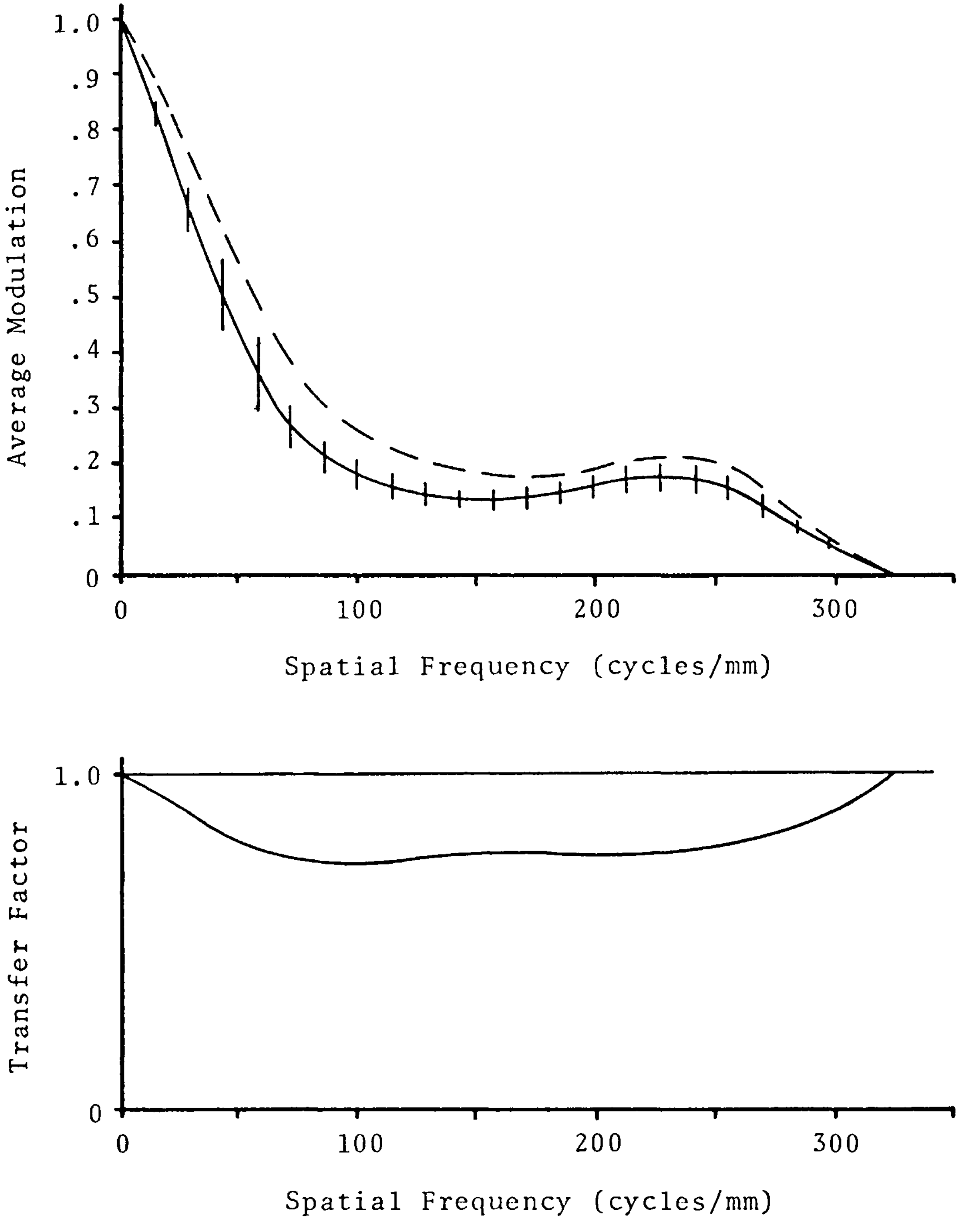

Fig. 29. Average Sagittal MTF at Full-Field for Error Group B.

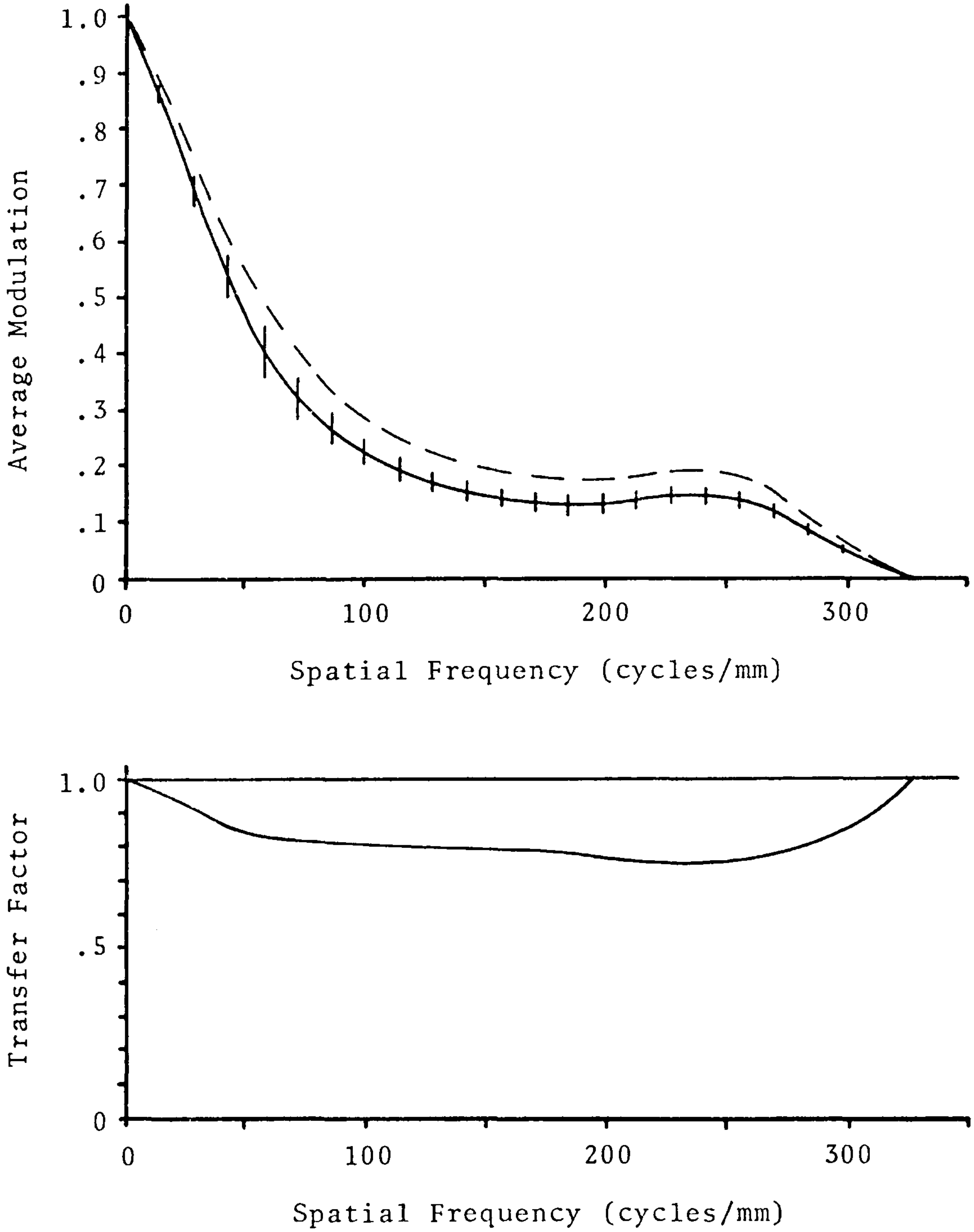

Fig. 30. Average Tangential MTF at Full-Field for Error Group B.

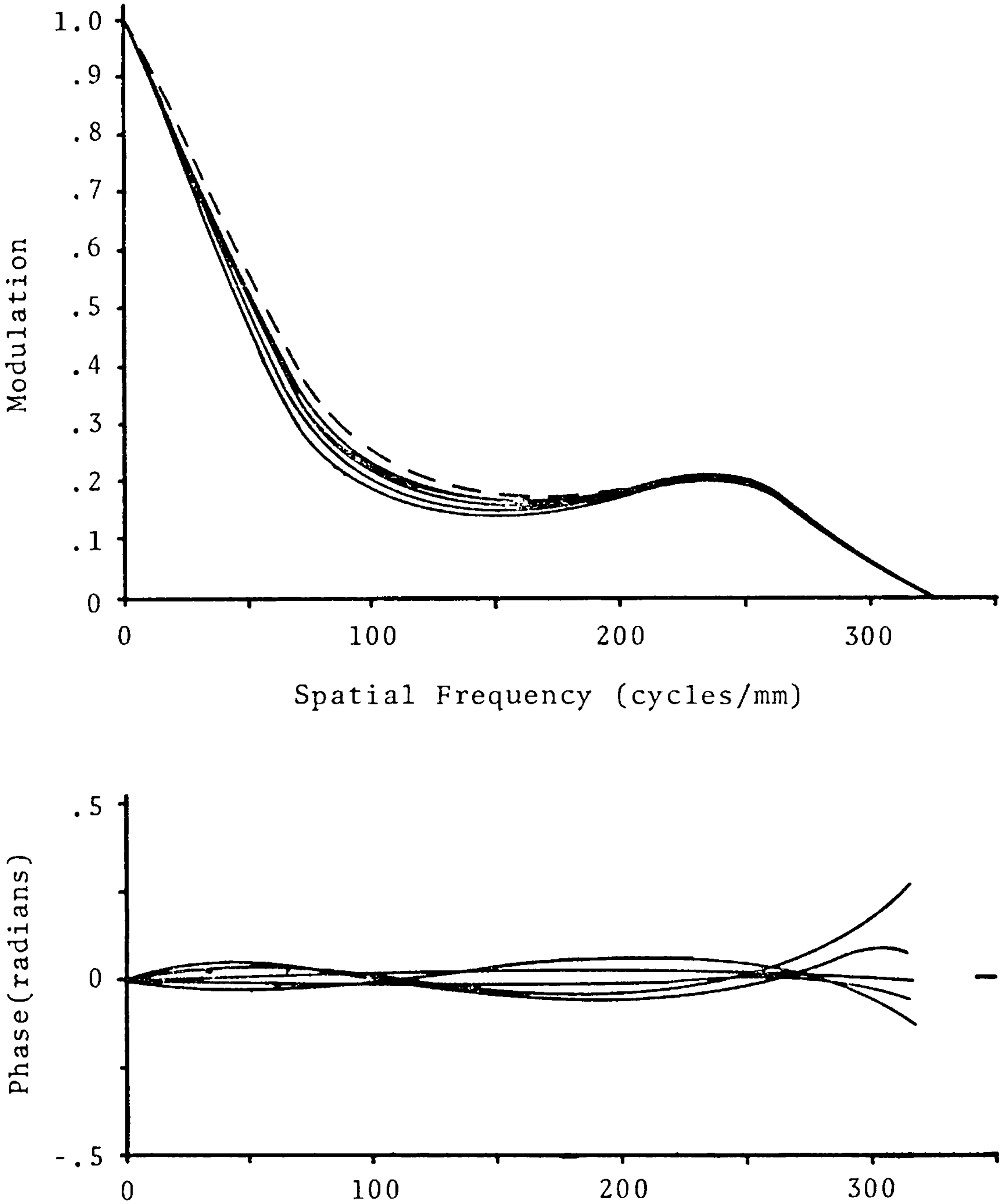

Fig. 31. Sagittal MTFs at Full-Field for Error Group C.

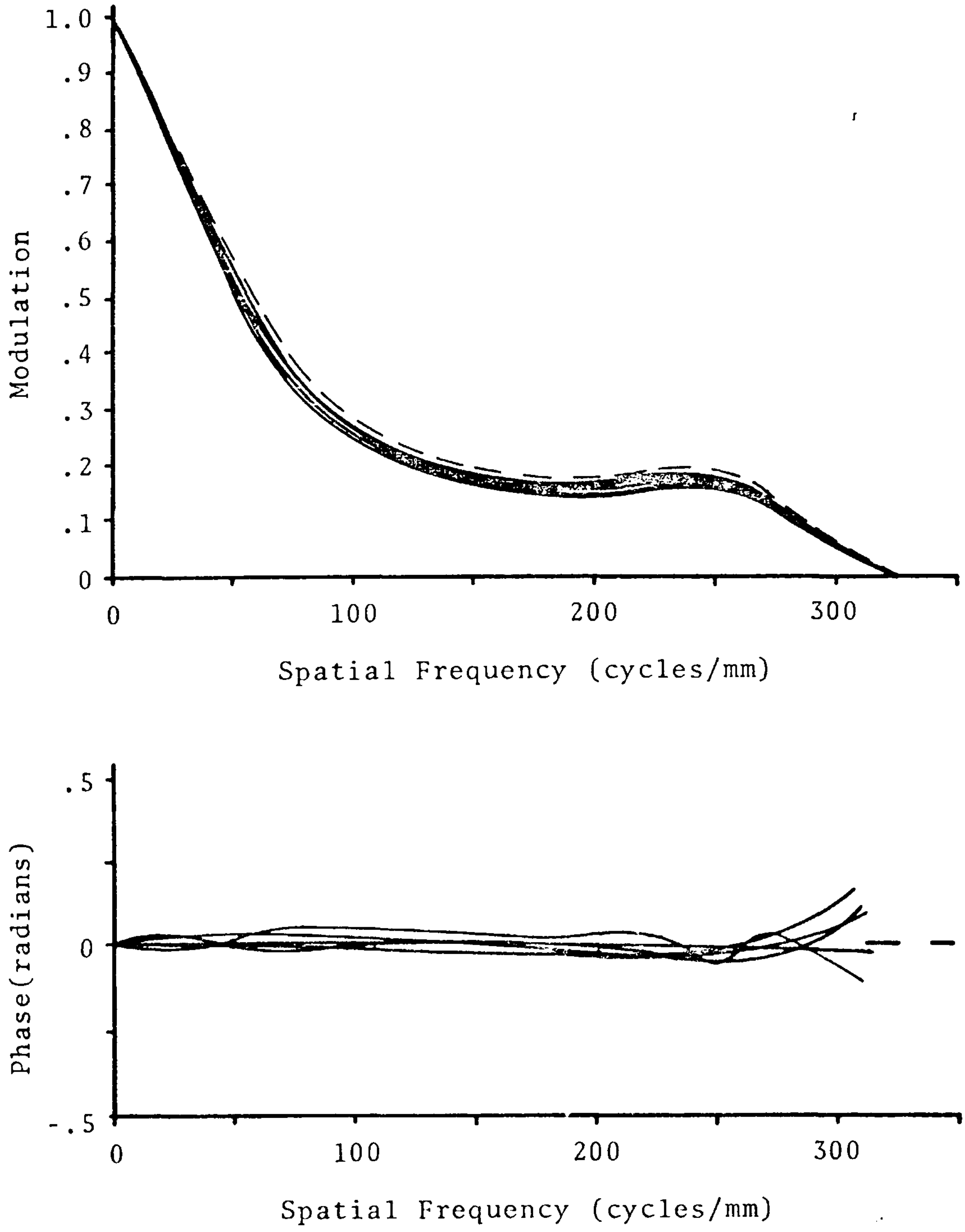

Fig. 32. Tangential MTFs at Full-Field for Error Group C.

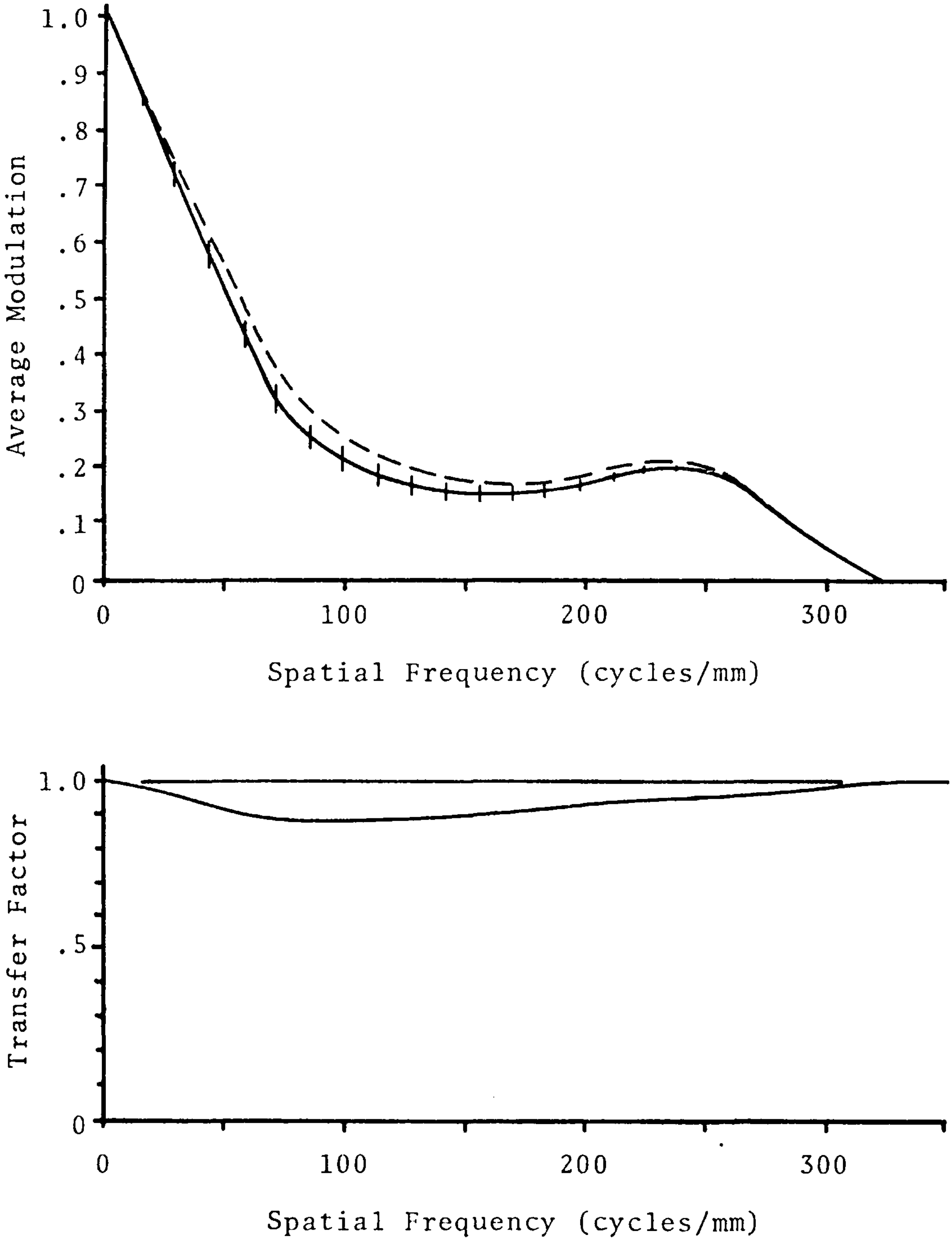

Fig. 33. Average Sagittal MTF at Full-Field for Error Group C.

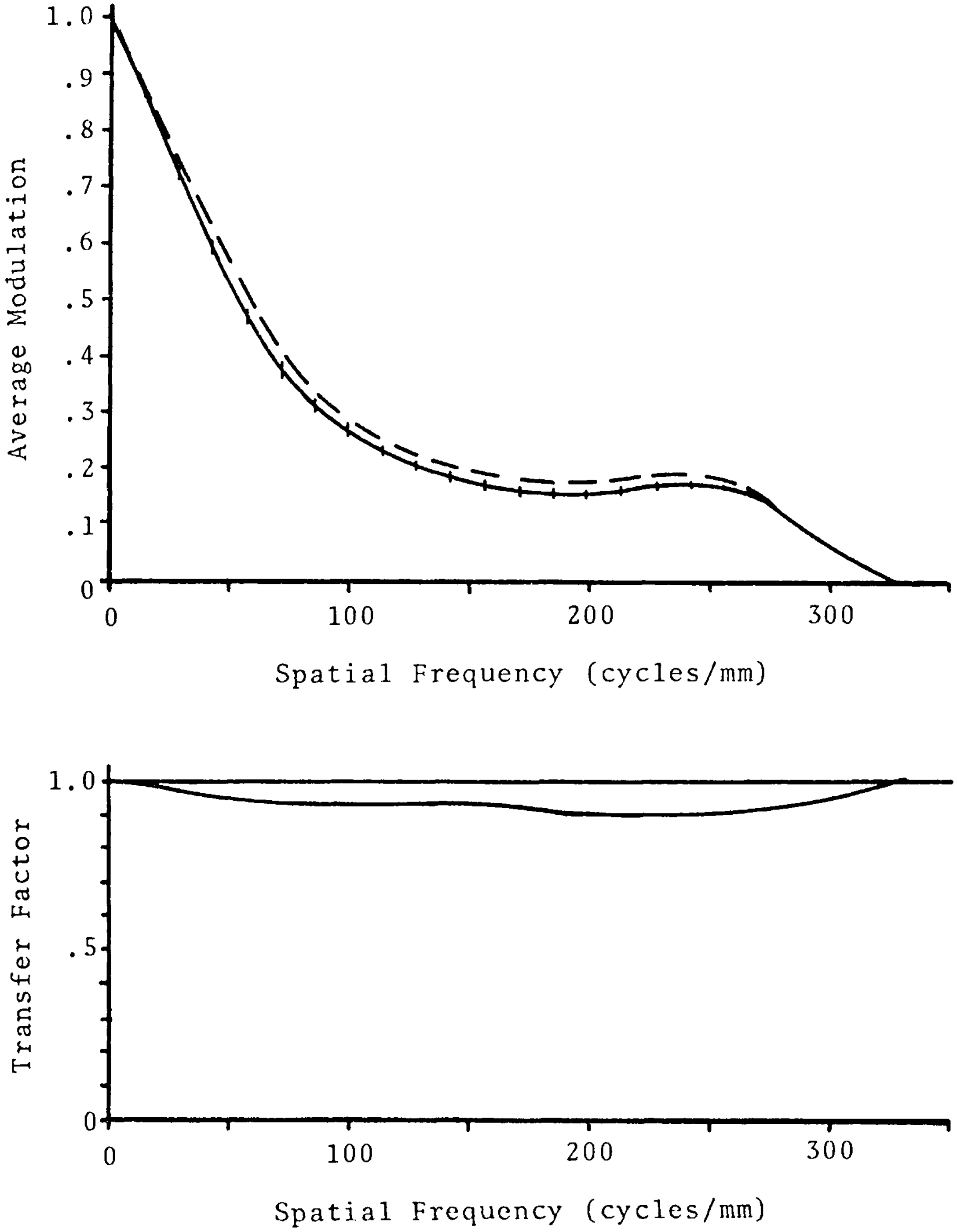

Fig. 34. Average Tangential MTF at Full-Field for Error Group C.

CHAPTER 8

CONCLUSIONS

From the preceding chapters, several conclusions can be made. These relate to the design of any three-mirror aspheric camera and to the expected performance of a fabricated system.

Selection of Minimum Diffracting Obscuration Ratio

In Figure 8, we see that for a given value of δ, the minimum value of the diffracting obscuration ratio, ρ_d, occurs where the curve, corresponding to that value of δ, crosses the dashed line. For any other points on the curve, the larger of the values ρ or ρ_{emin} is greater than ρ at the intersection point. The figure shows that as δ increases, the value of ρ at the intersection point also increases. Since the minimum acceptable value of δ is 0.25 inches, the minimum value of ρ_d occurs where the curve corresponding to δ equal to 0.25 inches crosses the dashed line. At this point,

$$\rho_d = \rho = 0.556 \ .$$

The value used for ρ_d in design C was

$$\rho_d = 0.5625 \ .$$

Therefore, design C, for all practical purposes, satisfies the requirement for a minimum diffracting obscuration ratio.

The procedure outlined in Chapter 5 successfully arrives at a design for the Meinel-Shack Three-Mirror Camera with a minimum diffracting ratio when the field angle, f-number, aperture and back focal distance are known.

Selection of Design C

Figures 18 through 22 show the modulation transfer functions of designs C and D. These show that the MTF of design D has a smaller modulus than that of C for spatial frequencies less than 250 cycles/millimeter. This relationship holds for both the sagittal and tangential directions and over the whole field.

Design C was selected as the better design for the reasons outlined above.

System Performance Within Different Error Groups

Figures 23 through 34 describe the effect of increasingly tighter tolerance specifications on the performance of fabricated systems. Error group C has a higher average modulus than B, and B has a higher average modulus than C. Also the spread of the moduli for individual systems is smallest for group C and largest for group A.

The phase in error groups B and C does not fluctuate very much. The maximum amplitude has a value of about 0.1 radians. The phase in error group A fluctuates wildly. In one case, the large fluctuation made it impossible to plot the phase. Shifts less than $\pi/10$ radians will cause a very slight blurring of the imagery and can generally be ignored. This is especially true of the higher spatial frequencies which have lower amplitudes. Therefore, the phase shifts in groups B and C can be ignored. However, the large phase shifts in error group A will degrade the imagery.

The transfer factors which are plotted in Figures 25, 26, 29, 30, 33, and 34 show that the major effect of manufacturing errors, on the MTF, occurs at the midfrequencies. The transfer factor, plotted as a function of spatial frequency, is relatively flat from 75 cycles/mm to 250 cycles/mm.

Because of the low average modulus, the large spread in the individual moduli and the rapid phase changes, construction of a system with the tolerances of group A should not be attempted. Construction of a system with the tolerances of groups B and C would result in one which closely approaches the theoretical maximum.

Predicted Resolution

Table V shows the predicted resolution for three types of emulsions. Included are values for the average MTF in each error group and values for the lowest MTF. As an example, the resolving power of the lowest MTF in the sagittal direction for error group B is 55 cycles/mm when used with type 4401 emulsion.

TABLE V

Predicted Resolving Power (cycles/mm)

Group	Plot	Direction	Emulsion Type 4401	Emulsion Type SO-206	Emulsion Type 4404
A	Average	Sagittal	45	80	120
		Tangential	55	90	125
	Lowest	Sagittal	25	50	65
		Tangential	30	45	55
B	Average	Sagittal	60	120	225
		Tangential	70	125	180
	Lowest	Sagittal	55	100	140
		Tangential	60	115	160
C	Average	Sagittal	72	125	250
		Tangential	77	135	210
	Lowest	Sagittal	70	120	250
		Tangential	75	130	185

APPENDIX A

REVIEW OF $y,\bar{y}$ DIAGRAMS

The method of using $y,\bar{y}$ diagrams for first order design has been found by Delano to be a direct and time saving tool in the early stages of design for an optical system. It is used extensively in this report to arrive at results which would have been difficult to achieve by better known means. Determination of the system with the lowest possible obscuration ratio is one example of these results.

For any axially symmetric optical system, it is possible to find a paraxial skew ray whose projection in the xz plane is a marginal ray and whose projection in the yz plane is a chief ray. The skew ray strikes any plane surface which is normal to the optic axis at a point whose coordinates are x and y. If we relable the x axis as $\bar{y}$, then these coordinates give the chief and marginal ray heights at the surface. Knowledge of the y and $\bar{y}$ values of a system uniquely determines an optical system.

We construct a rectangular coordinate system as in Figure 2. The horizontal axis is labeled $\bar{y}$ and the vertical is y. We can plot the y and $\bar{y}$ values of the skew ray as it travels through space. This is like observing the projection of the skew ray on a $\bar{y},y$ plane. In common optical systems the skew ray is a straight line which changes direction only when meeting a surface with some power. For an object at a large distance to the left of the optical system, the marginal ray height will be constant near the system. This is shown by line A'A in Figure 2. Notice that the $\bar{y}$ height is negative and decreasing in size. When the skew ray strikes the primary, it will have its direction changed. Also, the direction of its $y,\bar{y}$ projection will change. This is shown by line AB. The coordinates of the intersection of lines A'A and AB locate the primary on the $y,\bar{y}$ diagram. Positive surfaces will cause the figure to be concave toward the origin, and negative surfaces will cause the figure to be concave away from the origin. The point where the $y,\bar{y}$ projection crosses the y axis locates the stop of the system because, at the stop, $\bar{y}$ equals zero. The point where the plot crosses the $\bar{y}$ axis locates an image point, because here y equals zero. Generally, the $y,\bar{y}$ values at a surface are used to locate that surface on a $y,\bar{y}$ diagram.

From Delano, the axial distance between the two surfaces i and i + 1 is

$$d_{i\,i+1} = n_i' \frac{y_i\,\bar{y}_{i+1} - y_{i+1}\,\bar{y}_i}{H} .$$

Where $d_{i\,i+1}$ is the axial distance between the two surfaces, the index of refraction after the ith surface is n_i' and H is the Lagrange invariant.

The power, K_i, of the ith surface is given by

$$K_i = \frac{n_1'}{d_{i\,i+1}} \; \frac{(y_i - y_{i-1})(\bar{y}_{i+1} - \bar{y}_i) - (y_{i+1} - y_i)(\bar{y}_i - \bar{y}_{i+1})}{(y_{i-1}\,\bar{y}_i - y_i\,\bar{y}_{i-1})} \tag{A-1}$$

From these two equations, we see that we can find the powers of the surfaces and the spacings between them from knowledge of the $y, \bar{y}$ values, the indicies of refraction, and the Lagrange invariant.

Delano describes a convenient way to find the focal length of a lens. Figure 2 illustrates this method to find the focal length of the secondary. First, construct a line through the origin and parallel to the line AB. Next extend line BD until it crosses AB at point G. The distance which area OGB represents is equal to the focal length of the secondary.

$$f_2 = n_2' \frac{y_2\,\bar{y}_G}{H} \tag{A-2}$$

LIST OF REFERENCES

Brock, G. C., 1965, *Photographic Considerations for Aerospace*, Itek Corporation, Lexington, Mass., pp. 66-72.

Delano, Erwin, 1963, First-Order Design and the $y,\bar{y}$ Diagram, *Applied Optics* 2(12):1251-1256.

Shannon, R. R., Rudolph Kingslake ed., 1965, *Applied Optics and Optical Engineering*, Academic Press, New York, pp. 209-210.

Smith, Warren J., 1966, *Modern Optical Engineering*, McGraw-Hill, Inc., New York, pp. 248-257,322.